

*Appendix A***Supplementary Information for Chapter 2**

## A.1. Experimental section

### A.1.1 General Considerations

All manipulations were carried out using standard Schlenk or glovebox techniques under an N<sub>2</sub> atmosphere. Solvents were deoxygenated and dried by thoroughly sparging with N<sub>2</sub>, followed by passage through an activated alumina column in a solvent purification system by SG Water, USA LLC. Nonhalogenated solvents were tested with sodium benzophenone ketyl in tetrahydrofuran (THF) to confirm the absence of oxygen and water. Deuterated solvents were purchased from Cambridge Isotope Laboratories, Inc., degassed, and dried over activated 3-Å molecular sieves prior to use. [FeCN],<sup>1</sup> [FeCNMe<sub>2</sub>],<sup>1</sup> [P<sub>3</sub><sup>B</sup>Fe]BAr<sup>F</sup><sub>4</sub>,<sup>2</sup> PhB(*i*Pr<sub>2</sub>P)<sub>3</sub>FeBr,<sup>3</sup> [Ph<sub>2</sub>NH<sub>2</sub>]OTf,<sup>4</sup> KC<sub>8</sub>,<sup>1</sup> [H(OEt<sub>2</sub>)<sub>2</sub>]BAr<sup>F</sup><sub>4</sub>,<sup>5</sup> [TBA][<sup>13</sup>CN]<sup>6</sup> were synthesized using literature methods. (C<sub>6</sub>H<sub>6</sub>)<sub>2</sub>Cr, Cp\*<sub>2</sub>Cr and Cp<sub>2</sub>Co were purchased from Strem and used without further purification.

### A.1.2 Physical Methods

**NMR:** Nuclear Magnetic Resonance (NMR) measurements were recorded with a Varian 400 MHz spectrometer. <sup>1</sup>H NMR chemical shifts are reported in ppm relative to tetramethylsilane, using <sup>1</sup>H resonances from residual solvent as internal standards.<sup>7</sup>

**UV-Vis:** Ultraviolet-visible (UV-vis) absorption spectroscopy measurements were collected with a Cary 50 UV-vis spectrophotometer using a 1 cm path length quartz cuvette. All samples had a blank sample background subtraction applied. Temperature regulation for UV-Vis measurements was carried out with a Unisoku cryostat. Time course UV-Vis spectra were collected with the Scanning Kinetics application of the Cary WinUV software.

**Mössbauer spectra:** <sup>57</sup>Fe Mössbauer spectroscopy measurements were recorded on a spectrometer from SEE Co. (Edina, MN) operating in the constant acceleration mode in a transmission geometry. The sample was kept in an SVT-400 cryostat from Janis (Wilmington, MA). The quoted isomer shifts are relative to the centroid of the spectrum of a metallic foil of α-Fe at room temperature (RT). Solution samples were transferred to a sample cup, freeze-quenched with liquid nitrogen inside the glovebox,

and then immersed in liquid N<sub>2</sub> until mounted in the cryostat. Data analysis was performed using version 4 of the program WMOSS (wmoos.org), and quadrupole doublets fit Lorentzian lineshapes.

## **A.2 Ammonia production and quantification studies**

### **A.2.1 Standard NH<sub>3</sub> Generation Reaction Procedure**

All solvents are stirred with Na/K for  $\geq 2$  hours and filtered prior to use. In a nitrogen-filled glovebox, the precatalysts ([FeCN] or other Fe-complexes) are weighed in individual vials.\* The precatalysts are then transferred quantitatively into a Schlenk tube using benzene. The benzene is then lyophilized to provide a fluffy powder of precatalyst at the bottom of the Schlenk tube. The tube is then charged with a stir bar, and the acid ([Ph<sub>2</sub>NH<sub>2</sub>]OTf), reductant (e.g., (C<sub>6</sub>H<sub>6</sub>)<sub>2</sub>Cr) and [TBA][CN], all added as solids. The tube is sealed and cooled to 77 K in a cold well. To the cold tube 1 mL Et<sub>2</sub>O solvent is added to produce the desired precatalyst concentration. For reactions run above -20 °C additional Et<sub>2</sub>O was added taking into account the headspace of the tube and the vapor pressure of Et<sub>2</sub>O such that the reaction volume remained 1 mL. The temperature of the system is allowed to equilibrate for 5 minutes and then the tube is sealed with a Teflon screw-valve. This tube is passed out of the box into a liquid N<sub>2</sub> bath and transported to a fume hood. For experiments run at -78 °C, the tube is then transferred to a dry ice/isopropanol bath, where it thaws and is allowed to stir for a minimum of three hours before warming. For experiments run at -20 °C, the tube is instead transferred to a 3:1 ice:NaCl bath, where it thaws and is allowed to stir for a minimum of one hour before warming. For experiments run at 0 °C, the tube is transferred to an ice bath where it thaws and is allowed to stir for a minimum of three hours before warming. For experiments run at 25 °C, the tube is transferred to a water bath where it thaws and is allowed to stir for a minimum of 80 minutes. To ensure reproducibility, all experiments were conducted using 10 mm egg-shaped stir bars, and stirring was conducted at ~600 rpm.

\* In cases where less than 2.3  $\mu\text{mol}$  of precatalyst were used, stock solutions were used to avoid having to weigh very small amounts.

### A.2.2 NH<sub>3</sub> detection by <sup>1</sup>H NMR

Following the completed reaction, the reaction flask was cooled to 77 K and allowed to freeze. The reaction vessel is then opened to atmosphere and to the frozen solution is slowly added an excess KO<sup>t</sup>Bu as a solid (in at least two-fold excess with respect to acid) and THF (2 mL). This solution is allowed to freeze, then the headspace of the tube is evacuated, and the tube is sealed. The tube is then allowed to warm to RT and stirred at RT for at least 10 minutes. An additional Schlenk tube is charged with HCl (3 mL of a 2.0 M solution in Et<sub>2</sub>O, 6 mmol) to serve as a collection flask. The volatiles of the reaction mixture are vacuum transferred into this collection flask. After completion of the vacuum transfer, the collection flask is sealed and warmed to RT. Solvent is removed *in vacuo*, and the remaining residue is dissolved in a known amount of (1 mL or 0.5 mL) DMSO-*d*<sub>6</sub> containing 1,3,5-trimethoxybenzene as an internal standard. Integration of the <sup>1</sup>H NMR peak observed for NH<sub>4</sub><sup>+</sup> (δ 7.25 t, *J* = 52 Hz, 4H) is then integrated against the two peaks of 1,3,5-trimethoxybenzene to quantify the ammonium present. A typical spectrum is shown in Figure A.1. MeNH<sub>3</sub>Cl (when detected) is characterized in a similar fashion with the integration of diagnostic peaks (MeNH<sub>3</sub>Cl δ 7.78, br, 3H, δ 2.35, q, *J* = 8 Hz, 3H) against 1,3,5-trimethoxybenzene. A typical spectrum is shown in Figure A.2.

### A.2.3 Reload experiments

For the reload experiments (Table 2.1 entry 16), catalysis is set up as detailed in section A.1, except that following the sealing of the tube, it was allowed to thaw inside the glovebox and stirred for 80 minutes at 25 °C. After 80 minutes, the reaction mixture is filtered through a Celite pipette, with the flask and filter cake washed with an additional 2x(1 mL) dry Et<sub>2</sub>O. The extracted Et<sub>2</sub>O soluble products are added to a fresh Schlenk flask, and the solvent is removed *in vacuo*.

The (fresh) tube is then charged with a stir bar, the acid ([Ph<sub>2</sub>NH<sub>2</sub>]OTf), reductant ((C<sub>6</sub>H<sub>6</sub>)<sub>2</sub>Cr) and [TBA][CN]. The tube is sealed and cooled to 77 K in a cold well. To the cold tube Et<sub>2</sub>O is added, taking into account the headspace of the tube and the vapor pressure of Et<sub>2</sub>O such that the reaction volume remained 1 mL at 25 °C. The temperature of the system

is allowed to equilibrate for 5 minutes and then the tube is sealed with a Teflon screw-valve. This tube is passed out of the box into a liquid N<sub>2</sub> bath and transported to a fume hood. The reaction is warmed to room temperature and allowed to stir for 12 hours. The reloaded tube is analyzed as detailed in section A.2.2.

The first catalytic run is also analyzed for NH<sub>3</sub> (as detailed in section A.2.2), with the solids remaining on the Celite pipette being added back to the flask.

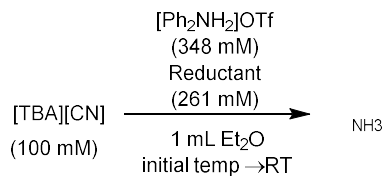
#### **A.2.4 A note on error bars and the solubility of species during catalysis**

Compared to similar N<sub>2</sub> reduction reactions, somewhat greater error between individual runs is observed.<sup>4,5</sup> We attribute this to the relative heterogeneity in the reaction mixture. [Ph<sub>2</sub>NH<sub>2</sub>]OTf is insoluble in Et<sub>2</sub>O, while [FeCN], (C<sub>6</sub>H<sub>6</sub>)<sub>2</sub>Cr and [TBA][CN] are all sparingly soluble. As a result, sufficient and consistent stirring was required to achieve reproducibility, but some variation was observed.

The relatively low catalyst solubility also necessitated the lyophilization of the precatalyst, particularly for low-temperature experiments. The increased surface area of lyophilized materials helps more rapidly solubilize the catalyst, which was found to be crucial to achieving efficient catalysis. Attempts to counteract these effects, e.g., by using THF for increased solubility, gave lower yields (Table A.1 runs A3 and B3), possibly due to a greater rate of background hydrogen evolution.

### A.2.5 NH<sub>3</sub> detection results

**Table A.1.** Catalytic yields for reduction of [TBA][CN] to yield NH<sub>3</sub>. <sup>a</sup>Assuming 6 e<sup>-</sup> reduction. <sup>b</sup>CH<sub>3</sub>NH<sub>2</sub> products also taken into account as a 4 e<sup>-</sup> product.



Entry	Catalyst loading (μmol) ([FeCN] is catalyst unless specified)	Conditions, ((C <sub>6</sub> H <sub>6</sub> ) <sub>2</sub> Cr is the reductant unless specified)	NH <sub>3</sub> (equiv/Fe)	Yield per reductant (%) <sup>a</sup>
A1	0.72 μmol	25 °C, Et <sub>2</sub> O	20.5	34.1
B1	0.72 μmol	25 °C, Et <sub>2</sub> O	32.8	54.6
C1	0.72 μmol	25 °C, Et <sub>2</sub> O	24.3	40.5
D1	0.72 μmol	25 °C, Et <sub>2</sub> O	32.5	54.2
<b>Table 2.1, entry 1</b>	<b>0.72 μmol</b>	<b>25 °C, Et<sub>2</sub>O</b>	<b>28±5</b>	<b>47±8</b>
E1	0.72 μmol	-20 °C, Et <sub>2</sub> O	27.6	46
F1	0.72 μmol	-20 °C, Et <sub>2</sub> O	43.4	72
<b>Table 2.1, entry 2</b>	<b>0.72 μmol</b>	<b>-20 °C, Et<sub>2</sub>O</b>	<b>35±8</b>	<b>58±13</b>
G1	0.72 μmol	0 °C, Et <sub>2</sub> O	27.6	46
H1	0.72 μmol	0 °C, Et <sub>2</sub> O	24.3	40.5
<b>Table 2.1, entry 3</b>	<b>0.72 μmol</b>	<b>0 °C, Et<sub>2</sub>O</b>	<b>26±2</b>	<b>43±3</b>
I1	0.72 μmol	-78 °C, Et <sub>2</sub> O,	16.2	23
J1	0.72 μmol	-78 °C, Et <sub>2</sub> O	39.0	55
K1	0.72 μmol	-78 °C, Et <sub>2</sub> O	30.7	44
L1	0.72 μmol	-78 °C, Et <sub>2</sub> O	46.2	66
<b>Table 2.1, entry 4</b>	<b>0.72 μmol</b>	<b>-78 °C, Et<sub>2</sub>O</b>	<b>33±6</b>	<b>55±10</b>
M1	2.9 μmol	-78 °C, Et <sub>2</sub> O	9.5	63
N1	2.9 μmol	-78 °C, Et <sub>2</sub> O	10.0	66
<b>Table 2.1, entry 5</b>	<b>2.9 μmol</b>	<b>-78 °C, Et<sub>2</sub>O</b>	<b>9.7±0.2</b>	<b>65±1</b>
O1	0.15 μmol	-78 °C, Et <sub>2</sub> O	76.5	25.5
P1	0.15 μmol	-78 °C, Et <sub>2</sub> O	69	23
<b>Table 2.1, entry 6</b>	<b>0.15 μmol</b>	<b>-78 °C, Et<sub>2</sub>O</b>	<b>73±4</b>	<b>24±1</b>

Entry	Catalyst loading ( $\mu\text{mol}$ ) ([FeCN] is catalyst unless specified)	Conditions, ( $(\text{C}_6\text{H}_6)_2\text{Cr}$ is the reductant unless specified)	$\text{NH}_3$ (equiv/Fe)	Yield per reductant (%) <sup>a</sup>
Q1	No catalyst	$-78\text{ }^\circ\text{C}$ , $\text{Et}_2\text{O}$	<0.05	<1
R1	No catalyst	$-78\text{ }^\circ\text{C}$ , $\text{Et}_2\text{O}$	<0.05	<1
<b>Table 2.1, entry 7</b>	<b>No catalyst</b>	<b><math>-78\text{ }^\circ\text{C}</math>, <math>\text{Et}_2\text{O}</math></b>	<b>&lt;0.05</b>	<b>&lt;1</b>
<b>S1 Table 2.1, entry 8</b>	<b>No [TBA][CN], [FeC<sup>15</sup>N] precatalyst</b>	<b><math>-78\text{ }^\circ\text{C}</math>, <math>\text{Et}_2\text{O}</math></b>	<b>0.7</b>	<b>1.1</b>
<b>T1 Table 2.1, entry 9</b>	<b><math>\text{FeCl}_2</math> 8 <math>\mu\text{mol}</math></b>	<b><math>-78\text{ }^\circ\text{C}</math>, <math>\text{Et}_2\text{O}</math></b>	<b>0.3</b>	<b>5.5</b>
<b>U1 Table 2.1, entry 10</b>	<b><math>\text{CrCl}_2</math> 8 <math>\mu\text{mol}</math></b>	<b><math>-78\text{ }^\circ\text{C}</math>, <math>\text{Et}_2\text{O}</math></b>	<b>&lt;0.03</b>	<b>&lt;0.5</b>
V1	$\text{PhB}(\text{CH}_2\text{Pr}_2\text{P})_3$ $\text{FeBr}$ (2.9 $\mu\text{mol}$ )	$-78\text{ }^\circ\text{C}$ , $\text{Et}_2\text{O}$	1.1 +0.4 $\text{MeNH}_2$ (equiv/Fe)	9.1
W1	$\text{PhB}(\text{CH}_2\text{Pr}_2\text{P})_3$ $\text{FeBr}$ (2.9 $\mu\text{mol}$ )	$-78\text{ }^\circ\text{C}$ , $\text{Et}_2\text{O}$	1.7 +0.85 $\text{MeNH}_2$ (equiv/Fe)	15.1
<b>Table 2.1, entry 11</b>	<b><math>\text{PhB}(\text{CH}_2\text{Pr}_2\text{P})_3</math> <math>\text{FeBr}</math> 2.9 <math>\mu\text{mol}</math></b>	<b><math>-78\text{ }^\circ\text{C}</math>, <math>\text{Et}_2\text{O}</math></b>	<b>1.4<math>\pm</math>0.7 +0.6<math>\pm</math>0.2 <math>\text{MeNH}_2</math> (equiv/Fe)</b>	<b>12<math>\pm</math>3<sup>b</sup></b>
X1	$[\text{P}_3^{\text{B}}\text{Fe}]\text{BAR}_4^{\text{F}}$ 2.9 $\mu\text{mol}$	$-78\text{ }^\circ\text{C}$ , $\text{Et}_2\text{O}$	2.2	14.7
Y1	$[\text{P}_3^{\text{B}}\text{Fe}]\text{BAR}_4^{\text{F}}$ 2.9 $\mu\text{mol}$	$-78\text{ }^\circ\text{C}$ , $\text{Et}_2\text{O}$	2.4	16.0
<b>Table 2.1, entry 12</b>	<b><math>[\text{P}_3^{\text{B}}\text{Fe}]\text{BAR}_4^{\text{F}}</math> 2.9 <math>\mu\text{mol}</math></b>	<b><math>-78\text{ }^\circ\text{C}</math>, <math>\text{Et}_2\text{O}</math></b>	<b>2.3<math>\pm</math>0.1</b>	<b>15.3<math>\pm</math>0.6</b>
Z1	0.72 $\mu\text{mol}$	$25\text{ }^\circ\text{C}$ , $\text{Et}_2\text{O}$ , $\text{Cp}_2\text{Co}$ reductant	3.6	6
A2	0.72 $\mu\text{mol}$	$25\text{ }^\circ\text{C}$ , $\text{Et}_2\text{O}$ , $\text{Cp}_2\text{Co}$ reductant	2.0	3.3

<b>Table 2.1, entry 13</b>	<b>0.72 <math>\mu\text{mol}</math></b>	<b>25 °C, Et<sub>2</sub>O, Cp<sub>2</sub>Co reductant</b>	<b>2.8<math>\pm</math>0.8</b>	<b>4.6<math>\pm</math>1.3</b>
----------------------------	--	---	-------------------------------	-------------------------------

Entry	Catalyst loading ( $\mu\text{mol}$ ) ([FeCN] is catalyst unless specified)	Conditions, ((C <sub>6</sub> H <sub>6</sub> ) <sub>2</sub> Cr is the reductant unless specified)	NH <sub>3</sub> (equiv/Fe)	Yield per reductant (%) <sup>a</sup>
B2	0.72 $\mu\text{mol}$	25 °C, Et <sub>2</sub> O, (Cp*) <sub>2</sub> Cr reductant	10.9	18.2
C2	0.72 $\mu\text{mol}$	25 °C, Et <sub>2</sub> O, (Cp*) <sub>2</sub> Cr reductant	16.1	26.8
<b>Table 2.1, entry 14</b>	<b>0.72 <math>\mu\text{mol}</math></b>	<b>25 °C, Et<sub>2</sub>O, (Cp*)<sub>2</sub>Cr reductant</b>	<b>13.5<math>\pm</math>3</b>	<b>22<math>\pm</math>5</b>
<b>D2, Table 2.1, entry 15</b>	<b>0.72 <math>\mu\text{mol}</math></b>	<b>25 °C, Et<sub>2</sub>O</b>	<b>32.4</b>	<b>54</b>
E2	0.72 $\mu\text{mol}$	25 °C, Et <sub>2</sub> O	3.1	5.2
F2	0.72 $\mu\text{mol}$	25 °C, Et <sub>2</sub> O	5.1	8.5
<b>Table 2.1, entry 16</b>	<b>0.72 <math>\mu\text{mol}</math></b>	<b>25 °C, Et<sub>2</sub>O</b>	<b>4.1<math>\pm</math>1</b>	<b>7<math>\pm</math>2</b>

*Additional catalytic runs*

Entry	Catalyst loading ( $\mu\text{mol}$ ) ([FeCN] is catalyst unless specified)	Conditions, ((C <sub>6</sub> H <sub>6</sub> ) <sub>2</sub> Cr is the reductant unless specified)	NH <sub>3</sub> (equiv/Fe)	Yield per reductant (%) <sup>a</sup>
A3	0.72 $\mu\text{mol}$	-78 °C, THF	12.3	
B3	0.72 $\mu\text{mol}$	-78 °C, THF	16.7	27.8
	0.72 $\mu\text{mol}$	<b>-78 °C, THF</b>	<b>14.5<math>\pm</math>2.2</b>	<b>24<math>\pm</math>4</b>
C3 <sup>c</sup>	2.9 $\mu\text{mol}$	-78 °C, Et <sub>2</sub> O	2.3	46
D3 <sup>c</sup>	2.9 $\mu\text{mol}$	-78 °C, Et <sub>2</sub> O	3.6	72
E3 <sup>c</sup>	2.9 $\mu\text{mol}$	-78 °C, Et <sub>2</sub> O	4.1	82
	2.9 $\mu\text{mol}$	<b>-78 °C, Et<sub>2</sub>O</b>	<b>3.3<math>\pm</math>0.6</b>	<b>66<math>\pm</math>12</b>

<sup>c</sup> loadings of 30 equiv (C<sub>6</sub>H<sub>6</sub>)<sub>2</sub>Cr (87 mM)/ 40 equiv [Ph<sub>2</sub>NH<sub>2</sub>]OTf (116 mM)/ 6 equiv [TBA][CN] (17.4 mM).

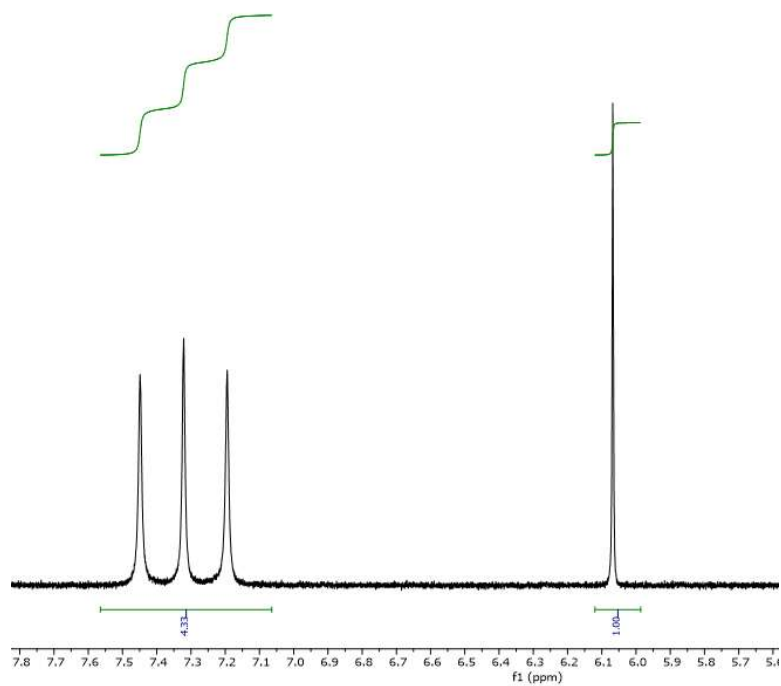


**Figure A.1.** Typical spectra for  $^1\text{H}$  NMR detection of  $[\text{NH}_4]\text{Cl}$  (triplet,  $J=52$  Hz at 7.31 ppm), with 10  $\mu\text{mol}$  1,3,5-trimethoxybenzene (TMB) added.

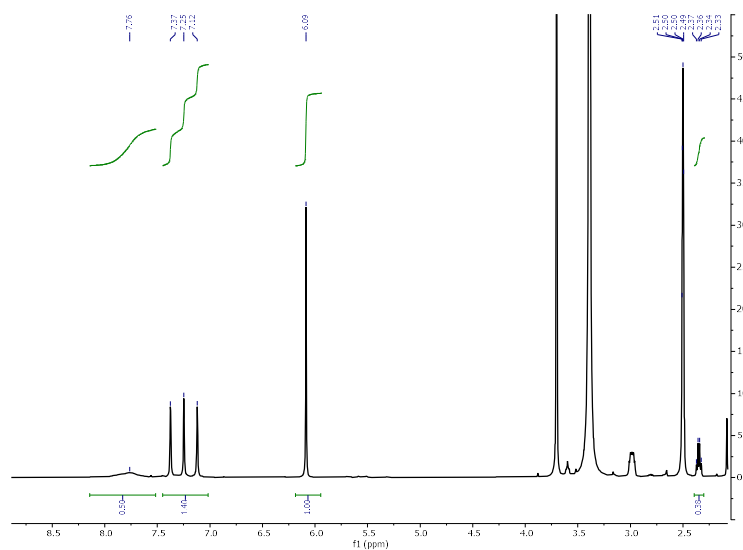


**Figure A.2.** Typical spectra for  $^1\text{H}$  NMR detection of  $[\text{NH}_4]\text{Cl}$  ( $\delta$  7.31 ppm (t),  $J=52$  Hz) and  $[\text{CH}_3\text{NH}_3]\text{Cl}$  ( $\delta$  7.78, br, 3H,  $\delta$  2.35, q,  $J = 8$  Hz, 3H), with 5  $\mu\text{mol}$  1,3,5-trimethoxybenzene (TMB) added.

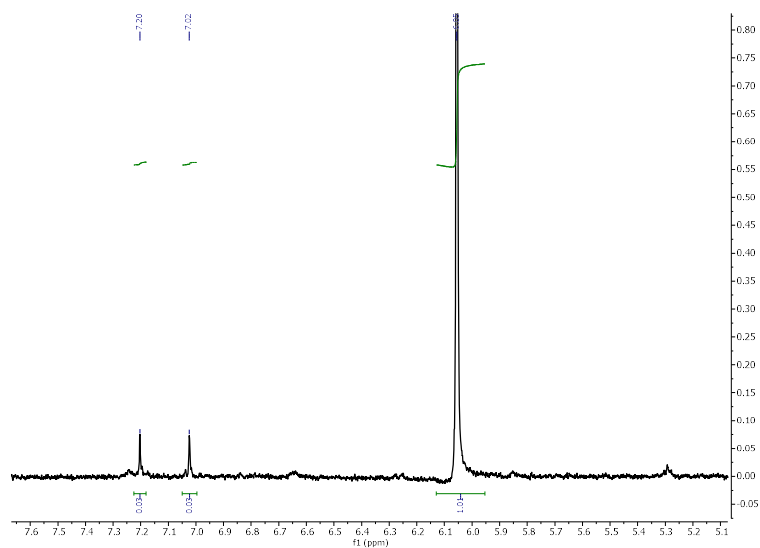


**Figure A.3.**  $^1\text{H}$  NMR detection of  $[\text{}^{15}\text{NH}_4]\text{Cl}$  ( $\delta$  7.1 ppm (d),  $J=72$  Hz) from reduction of  $[\text{FeC}^{15}\text{N}]$  (360 equiv  $(\text{C}_6\text{H}_6)_2\text{Cr}$  and 480 equiv  $[\text{Ph}_2\text{NH}_2]\text{OTf}$ ), in the absence of  $[\text{TBA}][\text{CN}]$ , quantified with 10  $\mu\text{mol}$  1,3,5-trimethoxybenzene (TMB) added. Lack of  $[\text{}^{14}\text{NH}_4]\text{Cl}$  rules out possible background  $\text{N}_2\text{R}$ .

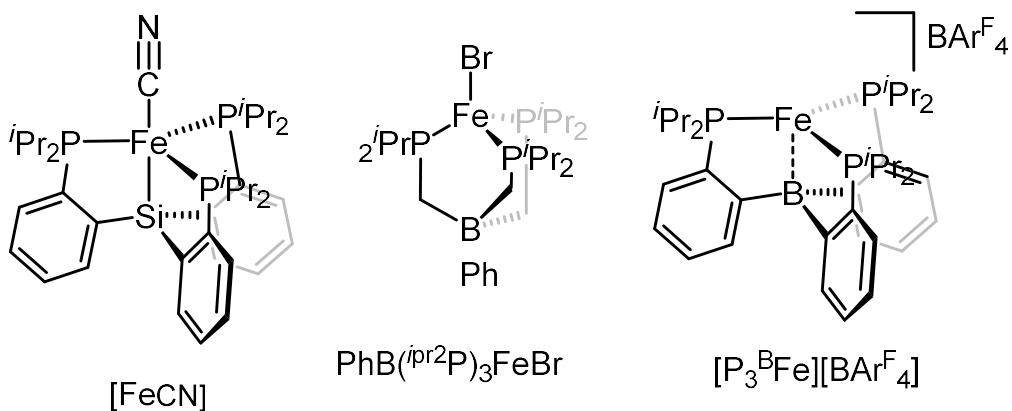


**Figure A.4.** Structures of molecular complexes employed as precatalysts.

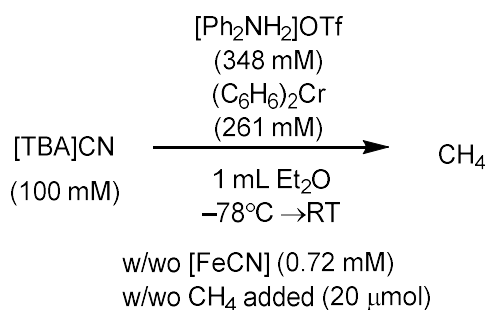
### A.3 Detection and quantification of gaseous products

#### A.3.1 General considerations

When using standard catalytic conditions, the acid, reductant and cyanide all constitute an appreciable wt% ([Ph<sub>2</sub>NH<sub>2</sub>]OTf wt. 12 %, (C<sub>6</sub>H<sub>6</sub>)<sub>2</sub>Cr wt. 6 % and [TBA][CN] wt. 4 %) of the reaction mixture and have an unknown effect on the solubility of gaseous organic products. We find that these reagents result in a greater amount of CH<sub>4</sub> absorbed in solution than expected for Et<sub>2</sub>O alone.

To initially quantify the amount of CH<sub>4</sub> produced, 4 tubes with chemical reagents ([TBA][CN], [Ph<sub>2</sub>NH<sub>2</sub>]OTf and (C<sub>6</sub>H<sub>6</sub>)<sub>2</sub>Cr, standard loadings table 1 entry 1) with and without [FeCN] (0.72 mM) and with and without 500 μL CH<sub>4</sub> added (at 25°C, 1 atm equals 20.5 μmol or 29.4 equiv per [Fe] at 0.72 mM catalyst loading) were prepared. After completion of the reaction, an aliquot from the headspace was injected on an HP 5890 GC-FID (30 M column length, 0.280 mm column diameter, He carrier gas), and the respective ratios of the CH<sub>4</sub> peak were compared (retention time=3.7 min). Using these measurements, the CH<sub>4</sub> yields were calculated (Table A.2). While we did not quantify C<sub>2</sub> products they were observed as possible minor components in the GC-FID, motivating the use of a gas analysis method on a different instrument that was previously calibrated for quantification of other gases C<sub>2</sub>H<sub>4</sub>, C<sub>2</sub>H<sub>6</sub>, and H<sub>2</sub>.

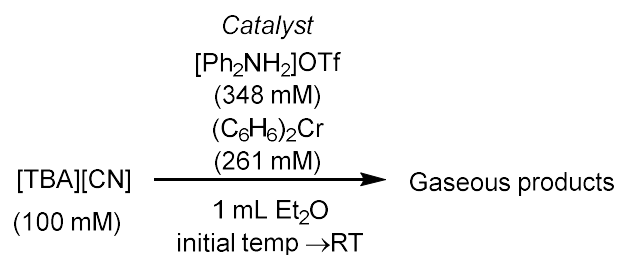
With the amount of CH<sub>4</sub> quantified, samples were manually injected on a combined GC-FID/TCD (SRI 8610C, in Multi Gas 5 configuration equipped with HayeSep D and Molsieve 5A columns). Hydrocarbons were detected by a S4 methanizer-flame ionization detector (FID), and the hydrogen was detected by a thermal conductivity detector (TCD). H<sub>2</sub>, C<sub>2</sub>H<sub>6</sub>, and C<sub>2</sub>H<sub>4</sub> were calculated with respect to CH<sub>4</sub> (Table A.3 and Table A.4). Using this same internal calibration, gaseous products from reactions run at room temperature and with the tris(phosphine) iron precatalysts were also quantified.

**Table A.2. Detection of CH<sub>4</sub> with control and leak test**

Sample	Signal Area CH <sub>4</sub>	Amount of CH <sub>4</sub> added	Amount of CH <sub>4</sub> detected	Amount of CH <sub>4</sub> produced
[Fe]	1754	0 μmol	22.3 μmol	22.0 μmol
[Fe] + 0.5 mL CH <sub>4</sub> (27.8 equiv)	3655	20 μmol	46.4 μmol	26.1 μmol
No Fe	28	0 μmol	0.3 μmol	
No Fe + 0.5 mL CH <sub>4</sub> (27.8 equiv)	1575	20 μmol	20 μmol	
			Average	24±2 μmol
				33±3 CH <sub>4</sub> per Fe

### A.3.2 Quantification of additional gases

To quantify the additional gaseous products observed, a GC-FID/TCD was used with a previously measured calibration curve. It was assumed that gas absorption (in the reaction mixture) was similar across gasses, as such the headspace gasses were used to calculate the ratios of H<sub>2</sub>/CH<sub>4</sub>, C<sub>2</sub>H<sub>4</sub>/CH<sub>4</sub>, and C<sub>2</sub>H<sub>6</sub>/CH<sub>4</sub>. This same internal calibration gaseous products at room temperature were also quantified in runs C and D, with <sup>Ph</sup>BP<sub>3</sub>FeBr precatalysts in runs D and E and P<sub>3</sub><sup>B</sup>Fe[BAr<sup>F</sup><sub>4</sub>] precatalyst in runs F.

**Table A.3. Summary of quantification of additional gaseous products.**

Catalyst (Loading)	Initial T	CH <sub>4</sub> equiv/Fe (yield%/Cr)	H <sub>2</sub> equiv/Fe (yield%/Cr)	C <sub>2</sub> H <sub>4</sub> equiv/Fe (yield%/Cr)	C <sub>2</sub> H <sub>6</sub> equiv/Fe (yield%/Cr)	C <sub>2</sub> /C <sub>1</sub> ratio
[FeCN] (0.575 mM)	-78°C	33±3 (55±5%)	53±15 (29±8%)	0.28±0.02 (0.6±0.04%)	0.21±0.02 (0.6±0.04%)	0.015
[FeCN] (0.575 mM)	25°C	27±4 (45±6%)	53±20 (29±11%)	0.33 (0.7%)	0.26±0.10 (0.7±0.3%)	0.022
<sup>Ph</sup> BP <sub>3</sub> FeBr (2.9 mM)	-78°C	1.0±0.1 (7.3±1%)	5.1±0.1 (11±0.2%)	0.09±0.01 (0.7±0.1%)	0.06±0.01 (0.8±0.1%)	0.11
P <sub>3</sub> <sup>B</sup> Fe[BAr <sup>F</sup> <sub>4</sub> ] (2.9 mM)	-78°C	1.6 (11%)	16 (36%)	0.1 (0.1%)	0.1 (0.1%)	0.16

**Table A.4.** Quantification of additional gases and room temperature catalysis.  
\*Headspace concentrations are relative based on GC-calibration.

Gas		CH <sub>4</sub>	H <sub>2</sub>	C <sub>2</sub> H <sub>4</sub>	C <sub>2</sub> H <sub>6</sub>
Run A (20 mL reaction volume)	Area	744	238	13.3	8.7
	Headspace concentration*	3250 ppm	4195 ppm	27 ppm	19.4 ppm
	Ratio to CH <sub>4</sub>	-	129%	0.8%	0.6%
Run B (20 mL reaction volume)	Area	762	366	15	10
	Headspace concentration*	3334 ppm	6485 ppm	31 ppm	22 ppm
		-	195%	0.9%	0.7%
Average ratio to CH <sub>4</sub>			162±46%	0.85±0.07%	0.65±0.07%
Yield per Fe		33±3	53±15	0.28±0.02	0.21±0.02
Yield per (C <sub>6</sub> H <sub>6</sub> ) <sub>2</sub> Cr		55±5	29±8%	0.6±0.04%	0.6±0.04%
<b>Room temperature gas analysis</b>					
Run C (150 mL reaction volume)	Area	118.9	108.7	2.4	0.6
	Headspace concentration*	406 ppm	995 ppm	4.6 ppm	2 ppm
	Ratio to CH <sub>4</sub> runs(A+B)	92%	220%	1%	0.5%
Run D (150 mL reaction volume)	Area	101.2	54.2	2.4	1.4
	Headspace concentration*	302 ppm	443 ppm	4.6 ppm	4.9 ppm
	Ratio to CH <sub>4</sub> (runs A+B)	70%	100%	1%	1.1%
Average ratio to CH <sub>4</sub>			160±60%	1%	0.8±0.3%

Yield per Fe		27±4	53±20	0.33	0.26±0.10
Yield per (C <sub>6</sub> H <sub>6</sub> ) <sub>2</sub> Cr		45±6	29±11%	0.7%	0.7±0.3%
<b>Gas</b>		<b>CH<sub>4</sub></b>	<b>H<sub>2</sub></b>	<b>C<sub>2</sub>H<sub>4</sub></b>	<b>C<sub>2</sub>H<sub>6</sub></b>
<b>Catalytic run with <sup>Ph</sup>BP<sub>3</sub>FeBr (2.9 mM)</b>					
Run E (20 mL reaction volume)	Area	105.3	109.7	19.4	9.2
	Headspace concentration*	360 ppm	2012 ppm	37 ppm	21 ppm
	Ratio to CH <sub>4</sub> runs(A+B)	11% (0.9 equiv)	61% (5 equiv)	1.1% (0.09 equiv)	0.6% (0.05 equiv)
Run F (20 mL reaction volume)	Area	127.7	114	19	10.8
	Headspace concentration*	434 ppm	2091 ppm	36 ppm	26 ppm
	Ratio to CH <sub>4</sub> (runs A+B)	13% (1.1 equiv)	64% (5.3 equiv)	1.1% (0.09 equiv)	0.8% (0.07 equiv)
Average ratio to CH <sub>4</sub>		12±1%	38.5±0.5%	1.1%	0.7±0.01%
Yield per Fe		1.0±0.1	5.1±0.1	0.09±0.01	0.06±0.01
Yield per (C <sub>6</sub> H <sub>6</sub> ) <sub>2</sub> Cr		7.3±1%	11±0.2%	0.7±0.1%	0.8±0.1%
<b>Catalytic run with (P<sub>3</sub><sup>B</sup>Fe)BAR<sup>F</sup><sub>4</sub> (2.9 mM)</b>					
Run G (20 mL reaction volume)	Area	182	356	21.6	12.5
	Headspace concentration*	622 ppm	6530 ppm	41.2 ppm	43.9 ppm
	Ratio to CH <sub>4</sub> runs(A+B)	19% (1.6 equiv)	198%	1.2%	1.3%
Yield per Fe		1.6	16	0.1	0.1
Yield per (C <sub>6</sub> H <sub>6</sub> ) <sub>2</sub> Cr		10.6%	36%	0.9%	1.1%

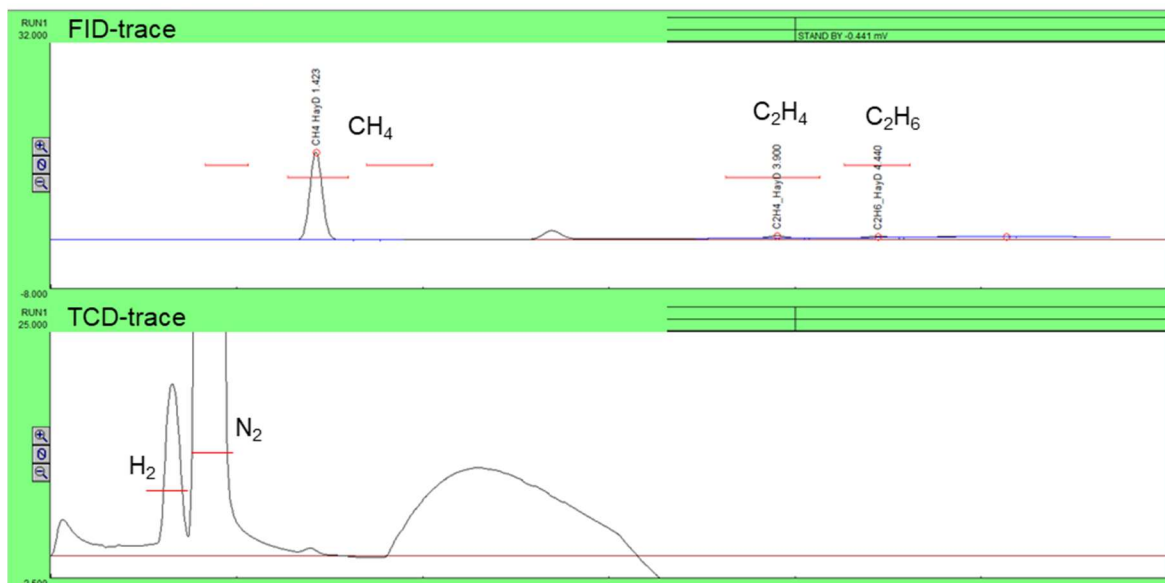


**Figure A.5.** Typical trace for GC-FID (top) and TCD (bottom) of gases detected, with CH<sub>4</sub>, C<sub>2</sub>H<sub>4</sub>, C<sub>2</sub>H<sub>6</sub> and H<sub>2</sub> highlighted.

## A.4 Additional control experiments

### A.4.1 Monitoring of [TBA]<sup>13</sup>CN consumption by NMR

To monitor the consumption of [CN]<sup>-</sup> and the formation of methane derived from [CN]<sup>-</sup>, [TBA][<sup>13</sup>CN] was used in a <sup>13</sup>C NMR experiment. Two J. Young NMR tubes were loaded with [TBA][<sup>13</sup>CN] (100 mM), (C<sub>6</sub>H<sub>6</sub>)<sub>2</sub>Cr (261 mM), and [Ph<sub>2</sub>NH<sub>2</sub>]OTf (348 mM); one of these tube was also loaded with [FeCN] (2.9 mM). The tubes were cooled to -78 °C, *d*<sub>8</sub>-THF was added, and the tubes were sealed. The tubes were allowed to warm up slowly with occasional mixing (by hand, every 10 minutes) for the first 2 hours of the reaction. Upon completion, analysis by <sup>13</sup>C NMR showed that only the tube loaded with [FeCN] had consumed <sup>13</sup>CN<sup>-</sup> and produced <sup>13</sup>CH<sub>4</sub>.

The use of THF was required to get sufficient solubility of reaction components, given the worse mixing in the J. Young tube. It was confirmed that setting up catalysis in THF still yields NH<sub>3</sub> (14.5±2.2, Table A.1, runs A3 and B3).

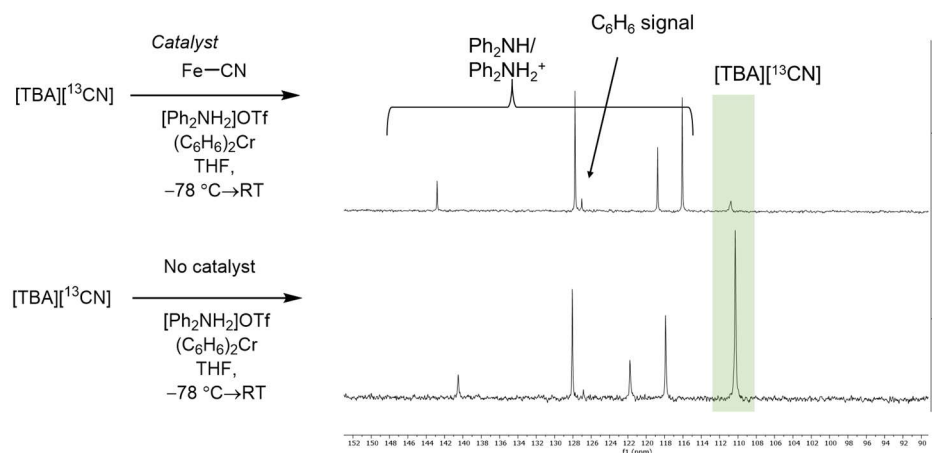


**Figure A.6.**  $^{13}\text{C}$  NMR spectra showing the reaction of  $[\text{TBA}][^{13}\text{CN}]$  with  $(\text{C}_6\text{H}_6)_2\text{Cr}$ ,  $[\text{Ph}_2\text{NH}_2]\text{OTf}$  in the presence and absence of  $[\text{FeCN}]$  catalyst. As compared to the peaks corresponding to  $\text{Ph}_2\text{NH}/[\text{Ph}_2\text{NH}_2]^+ [^{13}\text{CN}]^-$  is only appreciable consumed in the presence of  $[\text{FeCN}]$  (top spectrum).

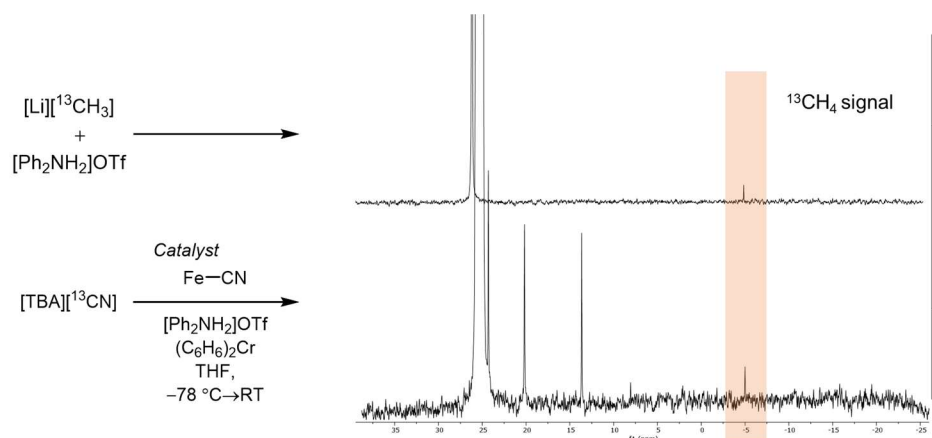


**Figure A.7.**  $^{13}\text{C}$  NMR spectra showing the reaction of  $[\text{TBA}][^{13}\text{CN}]$  with  $(\text{C}_6\text{H}_6)_2\text{Cr}$ ,  $[\text{Ph}_2\text{NH}_2]\text{OTf}$  in the presence of  $[\text{FeCN}]$  catalyst, with a  $^{13}\text{CH}_4$  peak ( $\delta - 4.8$  ppm, s), as compared to a sample generated upon the addition of acid to  $[\text{Li}][^{13}\text{CH}_3]$ .

#### A.4.2 Using $[\text{FeC}^{15}\text{N}]$ precatalyst.

To determine that the precatalyst  $\text{CN}^-$  ligand is consumed, we used  $[\text{FeC}^{15}\text{N}]$  labeled precatalyst but otherwise set up catalysis as usual (i.e., using natural abundance  $[\text{TBA}][\text{CN}]$ ). Low reactant loading conditions were used to not swamp out the  $^{15}\text{N}$  signal (2.9 mM  $\text{FeC}^{15}\text{N}$ , 6 equiv  $[\text{TBA}][\text{CN}]$ , 30 equiv  $(\text{C}_6\text{H}_6)_2\text{Cr}$ / 40 equiv  $[\text{Ph}_2\text{NH}_2]\text{OTf}$ ). 0.8 equiv  $[\text{NH}_4]^{15}\text{Cl}$  is detected along with about 3 equivalents  $[\text{NH}_4]^{14}\text{Cl}$  by  $^1\text{H}$  NMR, consistent with most of the

bound  $[\text{FeC}^{15}\text{N}]$  ligand being consumed. Catalysis with similar loading yielded similar amounts of  $\text{NH}_3$  (**Table A.1** entry C3-E3).

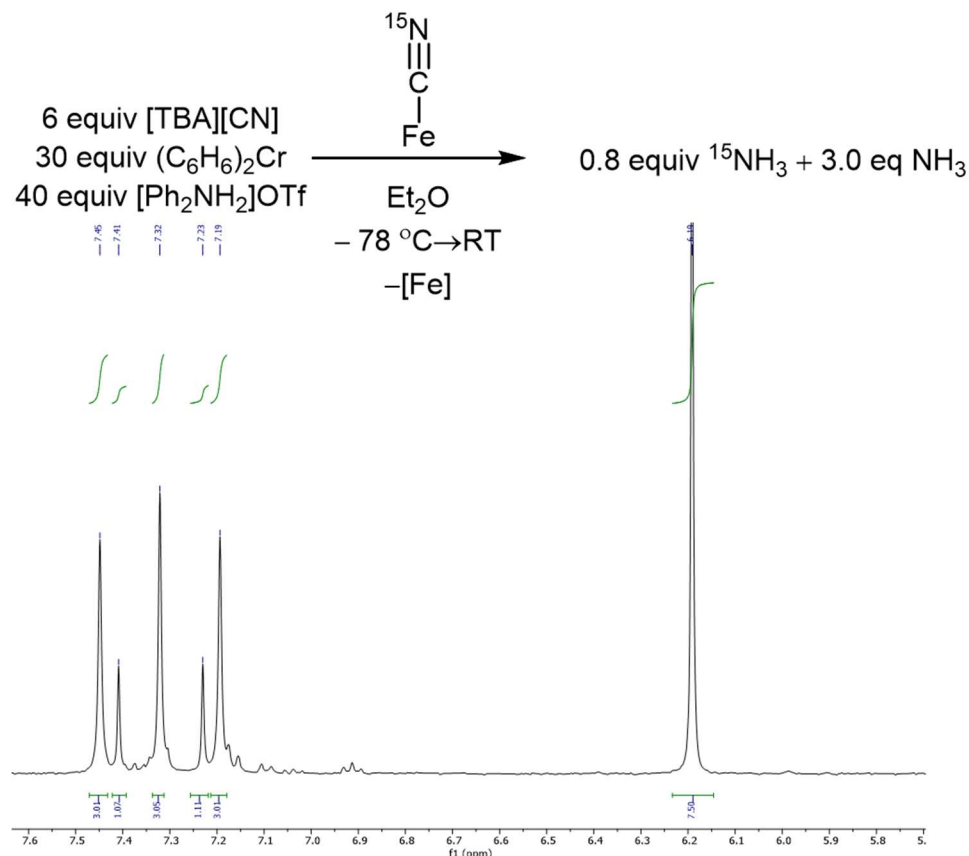


**Figure A.8.**  $^1\text{H}$  NMR detection of  $[\text{N}^{15}\text{NH}_4]\text{Cl}$  (triplet,  $J = 52$  Hz at 7.32 ppm), and  $[\text{N}^{15}\text{NH}_4]\text{Cl}$  (doublet,  $J = 72$  Hz at 7.32 ppm) with 10  $\mu\text{mol}$  1,3,5-trimethoxybenzene (TMB) added.

## A.5 Additional NMR experiments

### A.5.1 Stoichiometric reactions

#### A.5.1.1 Reduction of $[\text{FeCN}]$

$[\text{FeCN}]$  (2 mg, 2.9  $\mu\text{mol}$ ) was deposited in a Schlenk flask as a lyophilized powder, followed by the addition of  $(\text{C}_6\text{H}_6)_2\text{Cr}$  (3.6 mg, 6 equiv, 17.4  $\mu\text{mol}$ ) and  $[\text{Ph}_2\text{NH}_2]\text{OTf}$  (7.4 mg, 8 equiv, 23  $\mu\text{mol}$ ). The flask was cooled to  $-78^\circ\text{C}$ , and  $\text{Et}_2\text{O}$  (1 mL) was added via syringe. The flask was allowed to warm up slowly overnight and, after completion, was brought back into the glovebox. The solvent was removed *in vacuo*, and the contents were taken up in  $\text{C}_6\text{D}_6$  and analyzed by  $^1\text{H}$  NMR to find  $\text{P}_3\text{SiFeOTf}$  as the only detectable Fe-

species. In a separate experiment, the contents of the flask were worked up as described in section A.2.2.

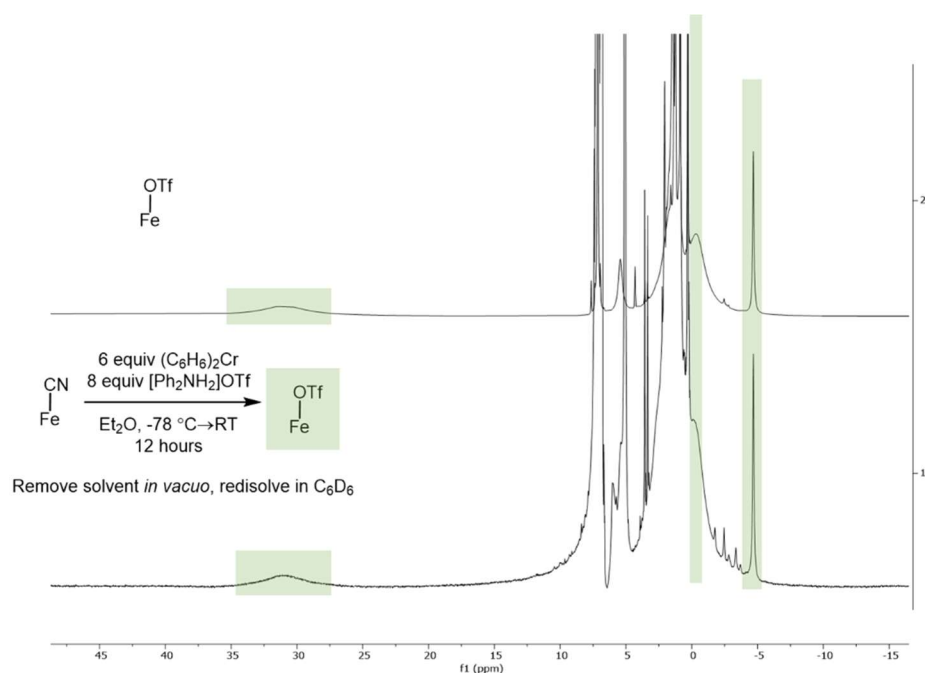


**Figure A.9.**  $^1\text{H}$  NMR of reaction of  $[\text{FeCN}]$  with 6 equiv  $(\text{C}_6\text{H}_6)_2\text{Cr}$  and 8 equiv  $[\text{Ph}_2\text{NH}_2]\text{OTf}$  in  $\text{Et}_2\text{O}$ . After completed reaction, solvent was removed *in vacuo* and the sample was redissolved in  $\text{C}_6\text{D}_6$ .  $^1\text{H}$  NMR showed that the  $[\text{Fe}]$  product was primarily  $[\text{FeOTf}]$ , green boxes for comparison to authentic sample.

#### A.5.1.2 Metathesis of $[\text{FeOTf}]$ to $[\text{FeCN}]$

$[\text{FeOTf}]^8$  (5 mg, 6  $\mu\text{mol}$ ) and  $[\text{TBA}][\text{CN}]$  (8.8 mg, 10 equiv, 60  $\mu\text{mol}$ ) were stirred in  $\text{Et}_2\text{O}$  at room temperature for 5 minutes, color change (orange to red) suggested a change in Fe-speciation consistent with  $[\text{FeCN}]$  formation. The solvent was removed *in vacuo*, and the contents were redissolved in  $\text{C}_6\text{D}_6$  to confirm  $[\text{FeCN}]$  formation by  $^1\text{H}$  NMR.  $^{19}\text{F}$  NMR showed mostly free  $\text{TfO}^-$  but some  $[\text{FeOTf}]$ .

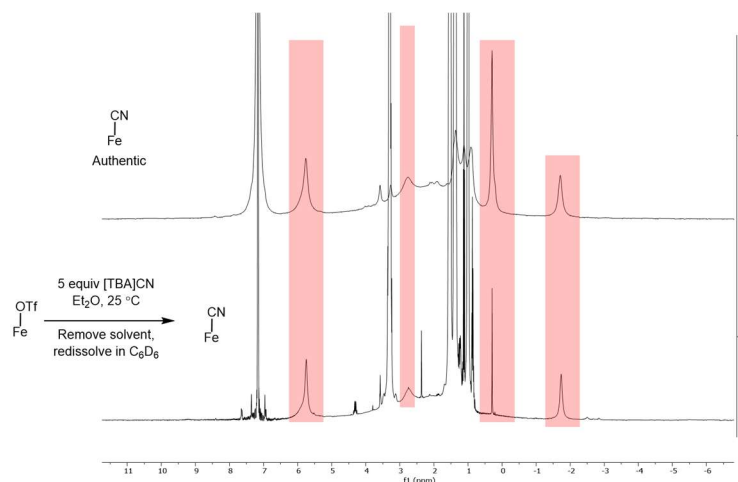


**Figure A.10.**  $^1\text{H}$  NMR of reaction of  $[\text{FeOTf}]$  with 10 equiv  $[\text{TBA}][\text{CN}]$  in  $\text{Et}_2\text{O}$ , stirred at  $25\text{ }^\circ\text{C}$  for 5 minutes at room temperature.  $^1\text{H}$  NMR showed that the  $[\text{Fe}]$  product was primarily  $[\text{FeCN}]$ , red boxes for comparison to authentic sample.

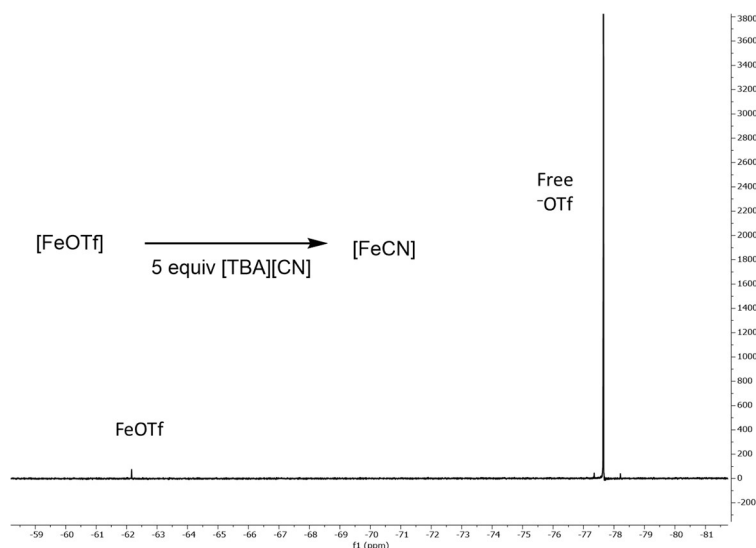


**Figure A.11.**  $^{19}\text{F}$  NMR of reaction of  $[\text{FeOTf}]$  with 10 equiv  $[\text{TBA}][\text{CN}]$  in  $\text{Et}_2\text{O}$ , stirred at  $25\text{ }^\circ\text{C}$  for 5 minutes at room temperature.  $^{19}\text{F}$  NMR showed that the  $^{19}\text{F}$ -product was primarily  $\text{TfO}^-$ .

### A.5.1.3 Reduction of $[\text{FeCN}]$ at room temperature

To confirm the assignment of  $[\text{FeOTf}]$  in Figure 2.3 (see main text), a parallel NMR experiment was run. In the glovebox,  $[\text{FeCN}]$  (2 mg,  $2.9\text{ }\mu\text{mol}$ ) was deposited in a J. Young tube as a lyophilized powder, followed by the addition of  $(\text{C}_6\text{H}_6)_2\text{Cr}$  (12 mg, 20 equiv,  $68\text{ }\mu\text{mol}$ ) and  $d_8\text{-THF}$  (0.6 mL).  $[\text{Ph}_2\text{NH}_2]\text{OTf}$  (22 mg, 20 equiv,  $68\text{ }\mu\text{mol}$ ) was added as a solid.

Within 5 minutes of acid addition, a  $^1\text{H}$  NMR of the reaction was collected, confirming the formation of  $[\text{FeOTf}]$ .  $\text{CH}_4$  and  $\text{NH}_3$  were confirmed in separate experiments, with the reaction being sampled or quenched after a 10-minute reaction time.

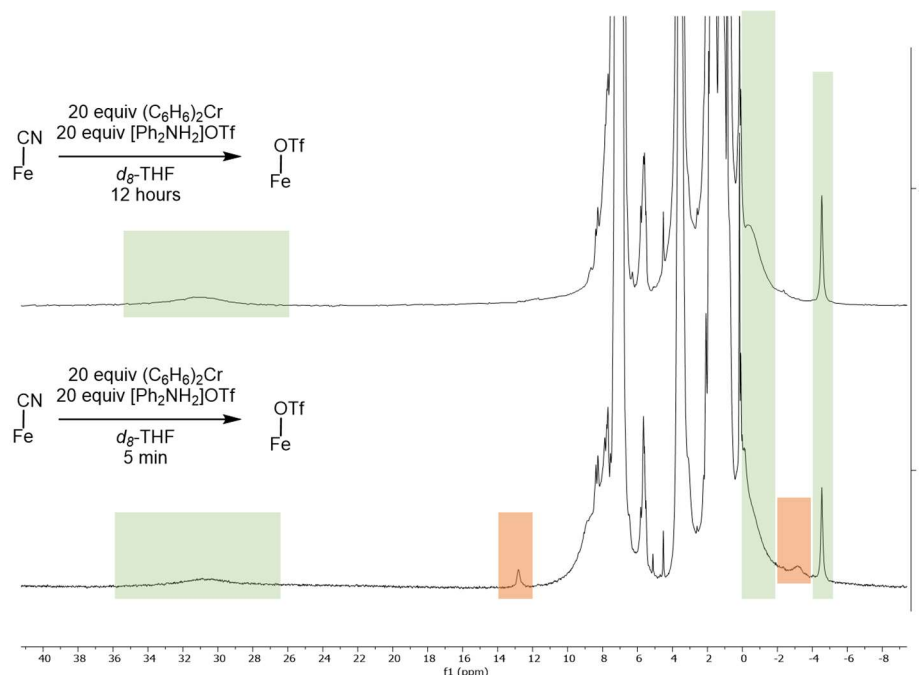
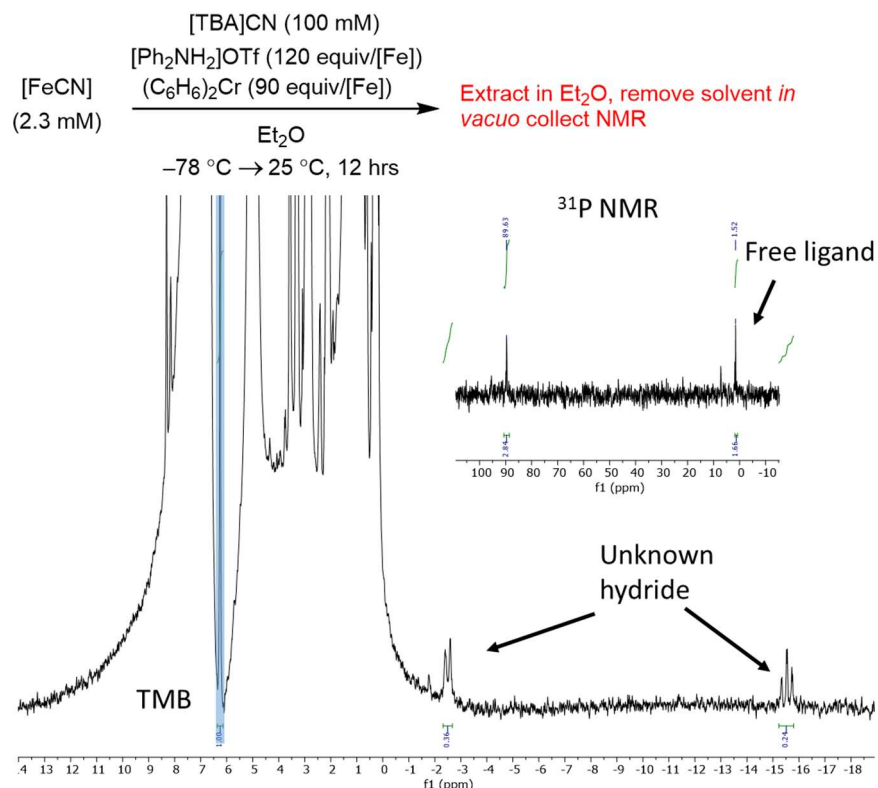


**Figure A.12.**  $^1\text{H}$  NMR of reaction of  $[\text{FeCN}]$  with 20 equiv  $(\text{C}_6\text{H}_6)_2\text{Cr}$  and 20 equiv  $[\text{Ph}_2\text{NH}_2]\text{OTf}$  in THF. After 5 minutes, multiple Fe-species are formed, including  $[\text{FeOTf}]$  and an unknown species (orange boxes). Overnight, this species disappears, and  $[\text{FeOTf}]$  is the only identifiable Fe-species.

### A.5.2 Analysis of post-catalysis products

Catalysis was setup as described in section 2.1. To more readily detect  $[\text{Fe}]$  products, the higher loadings (2.9 mM  $[\text{FeCN}]$ ; **Table 1**, entry 5) were used. After completed catalysis (12 hours), the reaction flask was brought back into the glovebox. The flask was filtered and extracted with additional  $\text{Et}_2\text{O}$ . The solvent was removed *in vacuo*, redissolved in  $\text{C}_6\text{D}_6$ , and analyzed. Fe–H species were detected, notably a doublet of triplets at  $\delta -15.5$  ppm. In addition, no  $[\text{FeOTf}]$  was observed (characteristic peaks  $\delta 31.5$ ,  $-4.5$  ppm were not observed).



### A.5.3 Stability measurements of other iron phosphine precatalysts

To assess possible reasons for poorer performance from the  $(\text{P}_3^{\text{B}})\text{Fe}[\text{BAr}^{\text{F}}_4]$  and  $(^{\text{Ph}}\text{BP}_3)\text{FeBr}$ , these catalysts (2.3 mM) were reacted with excess (20 equiv)  $[\text{TBA}][\text{CN}]$  in  $\text{Et}_2\text{O}$ . Analysis of the reaction mixture by  $^{31}\text{P}$  NMR after 15 minutes revealed free ligand from both precatalysts. In addition, a low spin Fe-bound product was observed upon the reaction of  $[\text{TBA}][\text{CN}]$  with  $^{\text{Ph}}\text{BP}_3\text{FeBr}$ , possibly arising from the formation of  $[\text{PhBP}_3\text{Fe}(\text{Br})(\text{CN})]^-$ .

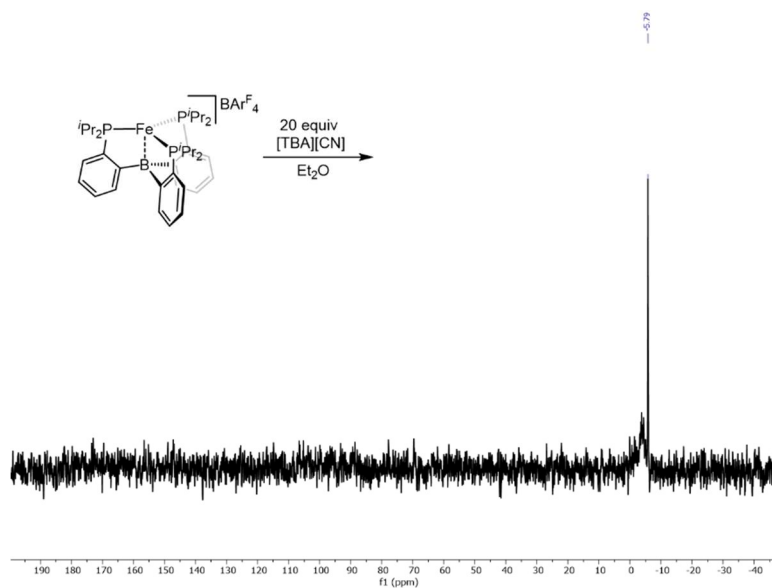


**Figure A.14.**  $^{31}\text{P}$  NMR of reaction of  $(\text{P}_3^{\text{B}})\text{Fe}[\text{BArF}_4]$  with  $[\text{TBA}][\text{CN}]$  in  $\text{Et}_2\text{O}$ . Sharp peak at  $-6.8$  ppm is consistent with unligated phosphine, with another broad peak ( $-3$  ppm) also observed.

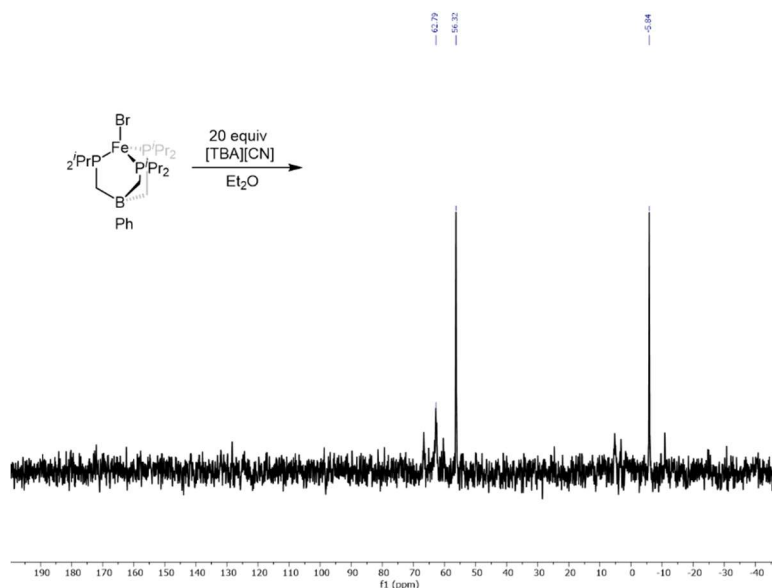


**Figure A.15.**  $^{31}\text{P}$  NMR analysis of reaction of  $(\text{PhBP}_3)\text{FeBr}$  with  $[\text{TBA}][\text{CN}]$  in  $\text{Et}_2\text{O}$ . Sharp peak at  $-5.9$  ppm is consistent with unligated phosphine. Another major peak at  $56.3$  ppm suggests the formation of diamagnetic Fe-species, perhaps from the formation of  $[\text{PhBP}_3\text{Fe}(\text{Br})(\text{CN})]^-$  or  $[\text{PhBP}_3\text{Fe}(\text{Br})(\text{CN})_2]^-$  with the  $\text{CN}^-$  ligand binding inducing a change of spin state from  $(\text{PhBP}_3)\text{FeBr}$  ( $S = 1$ ). Additional, small peaks are also observed ( $65$  ppm,  $63$  ppm,  $4$  ppm).

## A.6 Mössbauer data

### A.6.1 Note on the fitting of Mössbauer spectra

Data analysis was performed using version 4 of the program WMOSS ([www.wmoss.org](http://www.wmoss.org)), and quadrupole doublets fit Lorentzian lineshapes. Simulations were constructed from the minimum number of quadrupole doublets required to attain a quality fit to the data (convergence of  $\chi^2$ ). Quadrupole doublets were constrained to be symmetric. Using the non-linear error analysis algorithm provided by WMOSS, the errors in the computed parameters are estimated to be  $0.02 \text{ mm s}^{-1}$  for  $\delta$  and 2% for  $\Delta E_Q$ .

### A.6.2 Freeze-Quenched Mössbauer spectroscopy of catalytic reactions

#### A.6.2.1 General procedure for freeze-quenched catalytic reactions

All solvents are stirred with Na/K for  $\geq 2$  hours and filtered prior to use. In a nitrogen-filled glovebox, the desired  $^{57}\text{Fe}$  species (0.0023 mmol) is quantitatively transferred using benzene to a Schlenk flask and then lyophilized to yield a powder. That flask is charged with a stir bar and the other catalytic reagents as solids (analogous to catalytic reduction as described in section A.2.1). The tube is then chilled to 77 K in the glovebox cold-well and allowed to equilibrate for five minutes. To the chilled tube is added 1 mL of  $\text{Et}_2\text{O}$  and this flask is allowed to equilibrate for another five minutes. The flask is then transferred to a stir plate, where it is allowed to thaw. When the stir bar is freed from the frozen solvent and begins to stir the time is started. At the time noted, the stirring is stopped, and using a pipette, the reaction mixture is transferred in one portion to a Mössbauer cup sitting in a vial. The vial is then placed into the 77 K cooled cold well, allowing the reaction mixture to freeze in approximately twenty seconds. The sample is allowed to equilibrate for 20 minutes before being removed from the glovebox, immediately submerged in liquid nitrogen, and then mounted following standard procedure.

The resulting signals had broad  $^{57}\text{Fe}$  Mössbauer spectra, for which meaningful fits could not be readily generated. However, noting the chemistry of  $[\text{FeCN}]$  in the presence of excess  $[\text{Ph}_2\text{NH}_2]\text{OTf}$  and  $(\text{C}_6\text{H}_6)_2\text{Cr}$  (Figures 2.3 and A.12) and the known spectra of  $[\text{FeOTf}]$  ( $\delta = 0.66 \text{ mm s}^{-1}$ ,  $\Delta E_Q = <0.2 \text{ mm s}^{-1}$ , black line in figure A.14 is centered at 0.66

$\text{mm s}^{-1}$ ) we are reasonably confident that  $[\text{FeOTf}]$  is present at early times. NMR analysis of the mixtures at 80 minutes shows no evidence of  $[\text{FeOTf}]$  (Figure A.13).

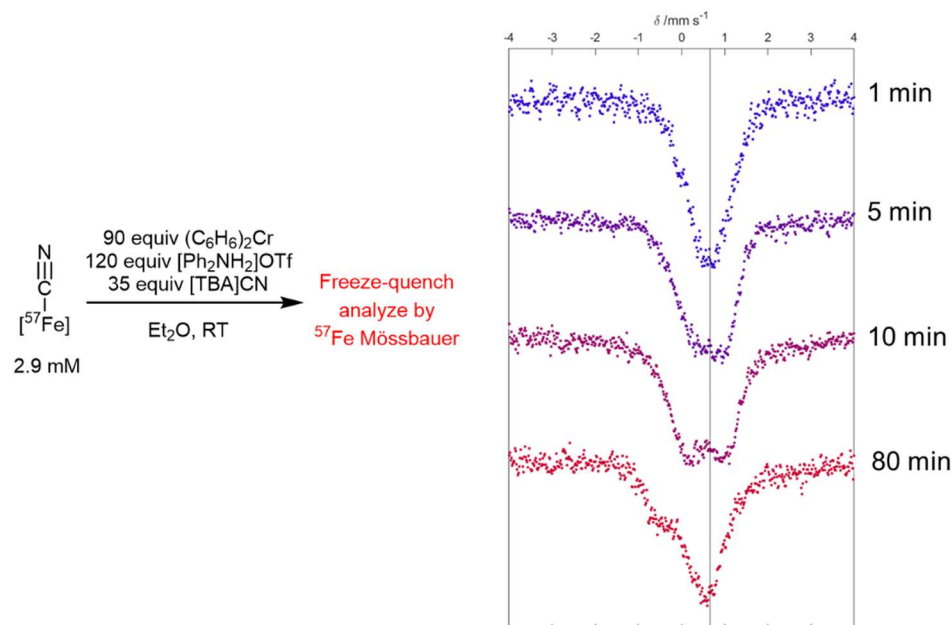
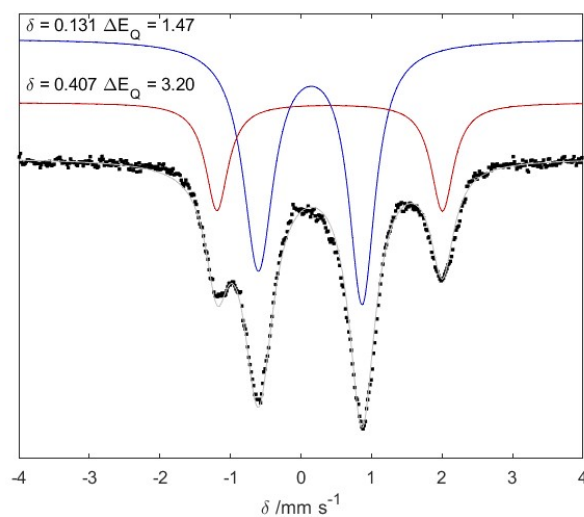


**Figure A.16.**  $^{57}\text{Fe}$  Mössbauer spectra of freeze-quenched catalytic reactions reacting  $[\text{FeCN}]$  (2.9 mM) with 90 equiv  $(\text{C}_6\text{H}_6)_2\text{Cr}$ , 120 equiv  $[\text{Ph}_2\text{NH}_2]\text{OTf}$  and 35 equiv  $[\text{TBA}][\text{CN}]$  in  $\text{Et}_2\text{O}$  for variable time.  $[\text{FeOTf}]$ , reported as a species with  $\delta = 0.66 \text{ mm s}^{-1}$ ;  $\Delta E_Q = <0.2 \text{ mm s}^{-1}$  is observed within 1 minute (Black line at  $0.66 \text{ mm s}^{-1}$ ).<sup>10</sup> Over time, other species appear, but we have not been able to assign them to known Fe-species.

### A.6.3 Mössbauer spectroscopy of reactions of $[\text{FeCN}]$ with reductant and acid

#### A.6.3.1 General Procedure for Freeze-Quenched Reactions

All solvents are stirred with Na/K for  $\geq 2$  hours and filtered prior to use. In a nitrogen-filled glovebox, the desired  $^{57}\text{Fe}$  species (0.0023 mmol) is dissolved in 0.3 mL  $\text{Et}_2\text{O}$  and cooled to  $-78^\circ\text{C}$  in a stirring vial in the glovebox cold well. Acid ( $[\text{Ph}_2\text{NH}_2]\text{BAr}^{\text{F}}_4$ , 0.00575 mmol) was added in 0.1 mL  $\text{Et}_2\text{O}$ . Reductant ( $(\text{C}_6\text{H}_6)_2\text{Cr}$  or  $\text{Cp}_2\text{Co}$ , 0.00575 mmol) was added in 0.3 mL to the chilled vial. The reaction was allowed to stir for 5 minutes before it was rapidly transferred to a pre-chilled Mössbauer cup. The cold well was then changed from  $-78^\circ\text{C}$  (195 K) to 77 K and the solution froze within 5 minutes. The Mössbauer cup was kept at 77 K for minimum 20 minutes before being rapidly taken out of the glovebox and submerged in liquid  $\text{N}_2$  and then mounted following standard procedure.



Trace	$\delta$ (mm s <sup>-1</sup> )	$\Delta E_Q$ (mm s <sup>-1</sup> )	Relative area	Assignment
Blue	0.13±0.01	1.47±0.01	71 %	[FeCNH <sub>2</sub> ] <sup>+</sup>
Red	0.41±0.01	3.20±0.01	29%	[FeCNH] <sup>+</sup>

**Figure A.17.** <sup>57</sup>Fe Mössbauer spectrum of reaction of [<sup>57</sup>FeCN] with 2.5 equiv each of (C<sub>6</sub>H<sub>6</sub>)<sub>2</sub>Cr and [Ph<sub>2</sub>NH<sub>2</sub>]<sup>F</sup>BAR<sup>F</sup><sub>4</sub>. Spectra fit as two species.

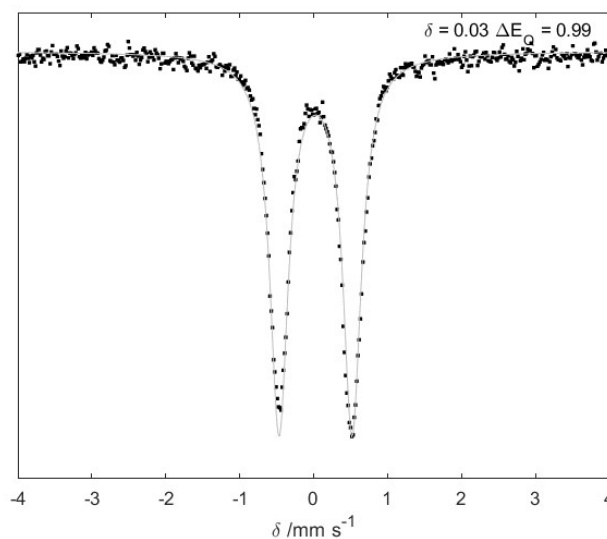


**Figure A.18.** <sup>57</sup>Fe Mössbauer spectrum of reaction of [<sup>57</sup>FeCN] with 2.5 equiv each of Cp<sub>2</sub>Co and [Ph<sub>2</sub>NH<sub>2</sub>]<sup>F</sup>BAR<sup>F</sup><sub>4</sub>. Spectra fit as a single species,  $\delta = 0.03 \pm 0.01$  mm s<sup>-1</sup>,  $\Delta E_Q = 0.99 \pm 0.01$  mm s<sup>-1</sup>.

## A.6.4 Alternative synthesis of [FeCNH<sub>2</sub>] Mössbauer sample

### A.6.4.1 Synthetic procedure

[FeCN] (20 mg, 29  $\mu\text{mol}$ ) was dissolved in 0.5 mL THF in a 20 ml vial. The solution was cooled to  $-78\text{ }^{\circ}\text{C}$ , and excess  $\text{KC}_8$  was added. The reaction mixture was then filtered through a pipette loaded with a filter paper, Celite, and  $\text{KC}_8$  3 times to form (proposed)  $[\text{FeCN}]\text{K}_2$ . The reaction mixture was filtered a final time to remove graphite and excess  $\text{KC}_8$ , giving a jet-black solution. This *in situ* formed material was used directly to form  $[\text{FeCNH}_2]$ . Alternatively, transferring this solution to a Mössbauer cup while maintaining the temperature, freezing the reaction mixture at 77 K, and analyzing by  $^{57}\text{Fe}$  Mössbauer revealed a Mössbauer spectrum with parameters  $\delta = 0.20\text{ mm s}^{-1}$ ,  $\Delta E_Q = 0.18\text{ mm s}^{-1}$  (Figure A.19 A), with a minor impurity.

For generation of  $[\text{FeCNH}_2]$ , 2 equiv  $[\text{H}(\text{OEt}_2)_2]\text{BAr}^{\text{F}}_4$  (59 mg, 58  $\mu\text{mol}$ ) dissolved in 0.3 mL THF, was added slowly to *in situ* formed  $[\text{FeCN}]\text{K}_2$ , with an orange solution formed. Transferring this solution to a Mössbauer cup while maintaining the temperature, freezing the reaction mixture at 77 K, and analyzing by  $^{57}\text{Fe}$  Mössbauer revealed a Mössbauer spectrum with parameters  $\delta = 0.02\text{ mm s}^{-1}$ ;  $\Delta E_Q = 0.96\text{ mms}^{-1}$  (Figure A.19 B), with some oxidized material also formed. The parameters of the major species fit those observed for  $[\text{FeCNH}_2]$  synthesized with  $[\text{Ph}_2\text{NH}_2]\text{BAr}^{\text{F}}_4$  and  $\text{Cp}_2\text{Co}$ .

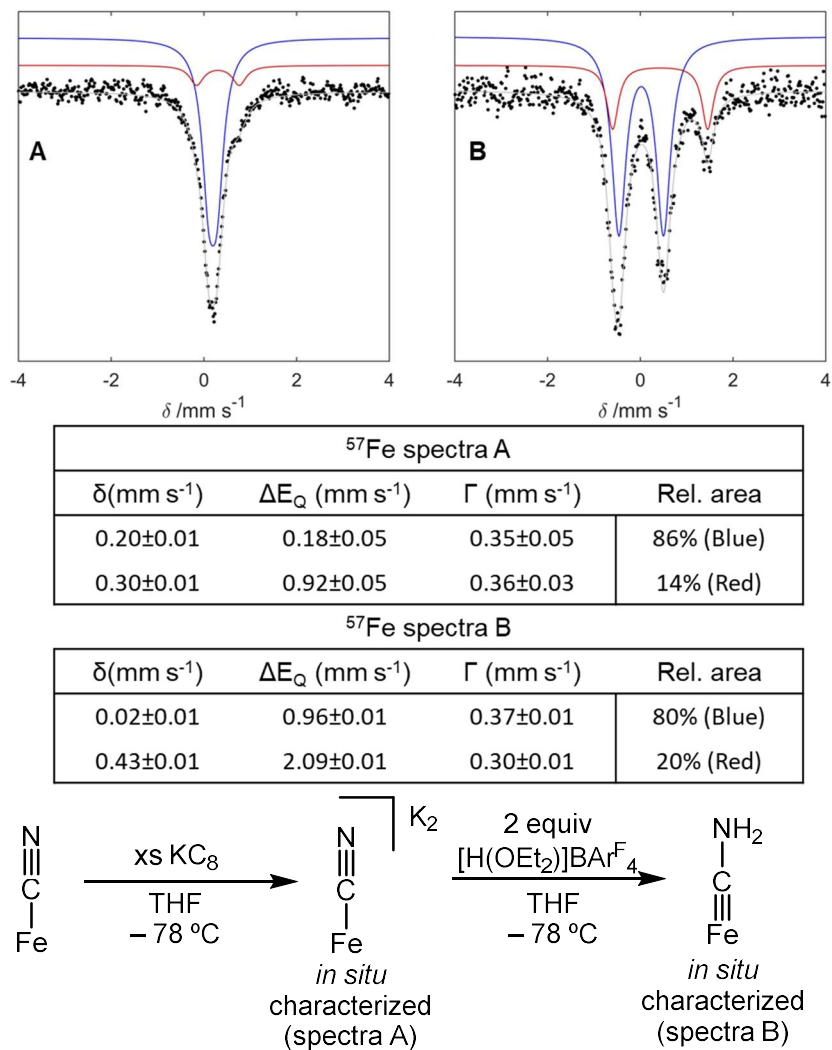


**Figure A.19.** <sup>57</sup>Fe Mössbauer of reaction of [<sup>57</sup>FeCN] with KC<sub>8</sub> (excess) to form proposed [<sup>57</sup>FeCN]K<sub>2</sub> (spectra A) and reaction of proposed [<sup>57</sup>FeCN]K<sub>2</sub> with 2 equiv [H(OEt<sub>2</sub>)<sub>2</sub>]BARF<sub>4</sub> to form [FeCNH<sub>2</sub>] (spectra B).

## A.7. UV-visible measurements

### A.7.1 General procedure for room temperature reduction of [FeCN] monitored by UV-vis spectroscopy

A 1 cm path length cuvette was loaded with [FeCN] (1 mM) and  $(C_6H_6)_2Cr$  (20 mM) in THF in the glovebox. The cuvette was sealed with a septum with  $N_2$  flowed through the septum to maintain an  $O_2$ -free atmosphere. To this solution,  $[Ph_2NH_2]OTf$  was rapidly added via syringe, and the reaction was monitored, collecting a spectrum every 6 seconds.

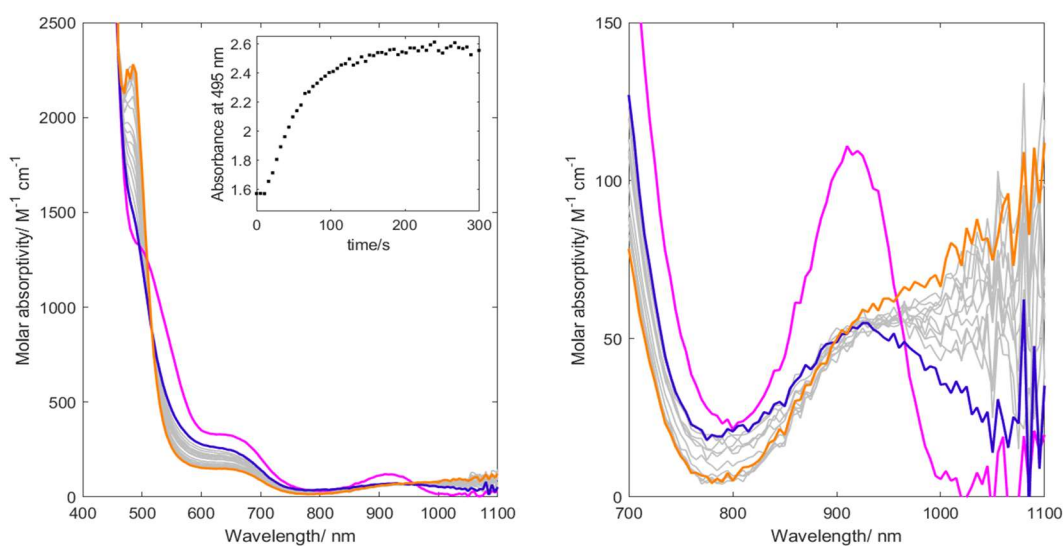


**Figure A.20.** Inset shows absorbance peak at 495 nm, which has previously been noted as characteristic for [FeOTf]. This peak grew in with a  $\tau_{1/2} = 40$  s. Zoomed out spectrum shows isosbestic point at 510 nm and sharp absorption at 495 nm characteristic of [FeOTf].

### A.7.2 General procedure for low-temperature UV-vis spectroscopy (Figure 2.4 B and C)

A 1 cm path length cuvette was loaded with [FeCN] (1 mM) in THF in the glovebox. It was sealed with a septum. It was brought out and allowed to equilibrate at the given temperature for 20 minutes. The temperature was maintained at  $-80^{\circ}C$ , with constant stirring during data collection. The acid was dissolved in 0.5 mL THF and added to the temperature-equilibrated cuvette. This resulted in the immediate formation of  $[FeCNH]^+$  (Figure A.21). Then, 2 equivalents of reductant were dissolved in 1 mL THF in the glovebox, brought out of the glovebox, and titrated into the solution via syringe. A spectrum was collected 2 minutes

after each addition of reductant. In the case of  $(C_6H_6)_2Cr$  an additional 4 equivalents of reductant were dissolved in an additional 1 mL of solvent to continue the titration. The spectra were plotted against molar absorptivity, adjusting for the change in concentration of  $[Fe]$  throughout the titration experiment (Figure 2.4B and C).

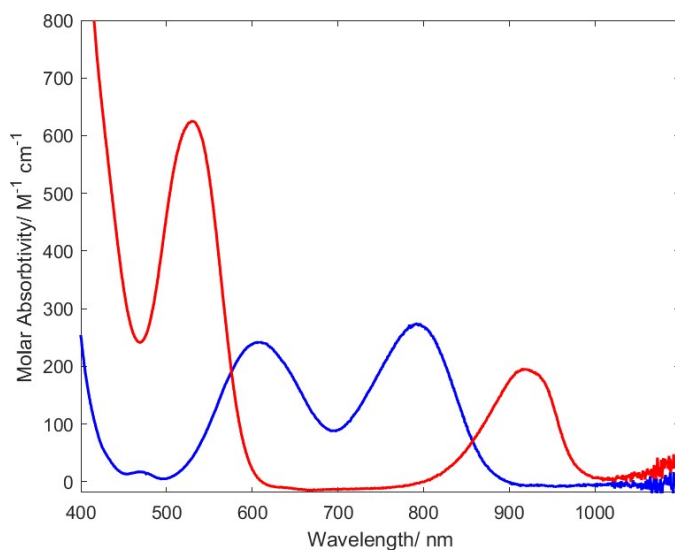


**Figure A.21.** UV-vis spectrum of starting  $[FeCN]$  (red) and after addition of  $[Ph_2NH_2]BARF_4$  (blue) in THF at  $-80\text{ }^\circ\text{C}$ . Features match what has been previously observed for  $[FeCN]$  and  $[FeCNH]^+$ .<sup>1,10</sup>

## A.8. Electrochemical measurements

### A.8.1 General procedure

Electrochemical measurements were conducted with a glassy carbon working electrode, a platinum wire counter electrode, and Ag/AgOTf (1mM AgOTf in 0.2 M [TBA][OTf]) reference electrode isolated by a CoralPor™ frit (obtained from BASi) and referenced externally to  $\text{Fc}^{+/0}$ . Unless otherwise specified, NaK dried THF was used as solvent, with 0.2 M [TBA]OTf electrolyte. Measurements were conducted with a CH Instruments 600B electrochemical analyzer.

### A.8.2 Acid reduction current with different reductants

To test the ability of each reductant to perform the hydrogen evolution reaction, we used electrochemical methods. Beginning the oxidized form of the reductants ( $[\text{red}]\text{BAr}^{\text{F}_4}$ ; red =  $(\text{C}_6\text{H}_6)_2\text{Cr}$ ,  $\text{Cp}_2\text{Co}$ ,  $\text{Cp}^*_2\text{Cr}$ ) for each  $[\text{red}]\text{BAr}^{\text{F}_4}$  the current associated with reduction is enhanced upon addition of  $[\text{Ph}_2\text{NH}_2]\text{OTf}$ . The increase in current is proposed to occur due to a catalytic EC mechanism (Figure A.20), with the reduction of  $[\text{red}]\text{BAr}^{\text{F}_4}$  followed by protonation and hydrogen evolution. The increase in current upon the addition of acid to each reductant becomes a measure of the rate of reaction between the reductant and  $[\text{Ph}_2\text{NH}_2]\text{OTf}$ , proposed to reflect the rate of background hydrogen evolution during catalysis.

$[\text{red}]\text{BAr}^{\text{F}_4}$  (Red =  $(\text{C}_6\text{H}_6)_2\text{Cr}$ ,  $\text{Cp}_2\text{Co}$ ,  $\text{Cp}^*_2\text{Cr}$ ) was prepared in an analogous way to  $[\text{Cp}^*_2\text{Co}]\text{BAr}^{\text{F}_4}$ <sup>11</sup> previously. 1 mM solutions were prepared in [TBA]OTf electrolyte (0.2 M) in THF. Acids were added as solids to avoid a change in concentration of  $[\text{red}]\text{BAr}^{\text{F}_4}$ .

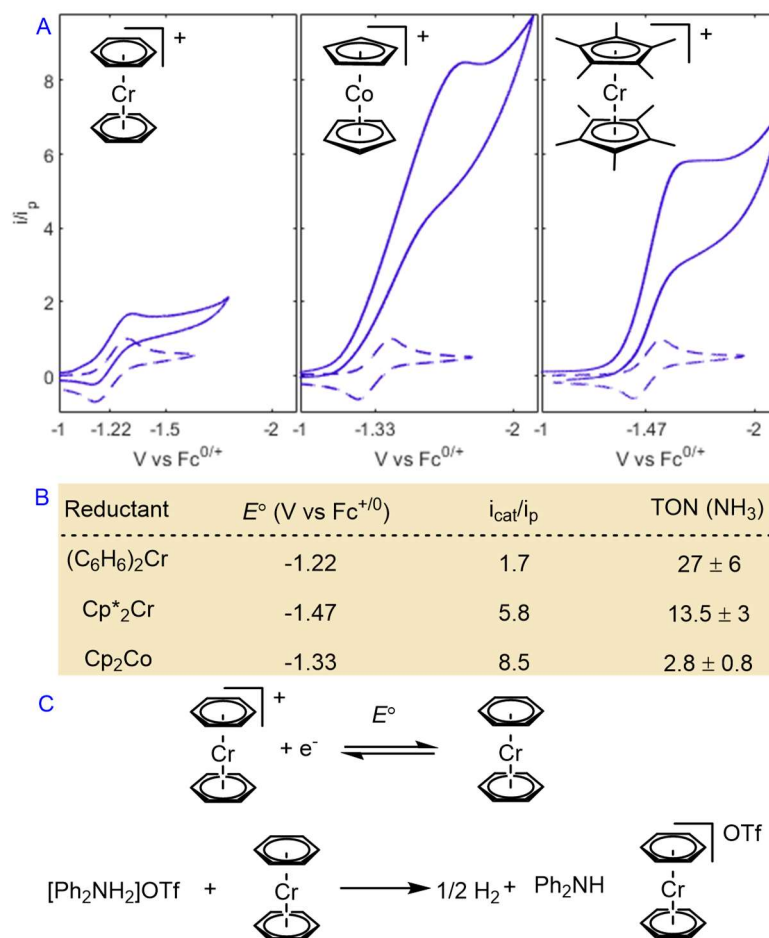


**Figure A.22.** Proton reduction by chemical reductants as measured by cyclic voltammetry. (A): Cyclic voltammograms of  $[\text{red}]\text{BAR}^{\text{F}}_4$  (1 mM) in 0.2 M  $[\text{TBA}]\text{OTf}$ , with 0 equiv  $[\text{Ph}_2\text{NH}_2]\text{OTf}$  (dashed) and 50 equiv  $[\text{Ph}_2\text{NH}_2]\text{OTf}$  (solid lines) ( $100 \text{ mV s}^{-1}$  scan rate). After addition of  $[\text{Ph}_2\text{NH}_2]\text{OTf}$  catalytic current is observed, but to a differing extent. The catalytic current measures the rate of reaction between acid and reductants. (B): Comparing the acid free current to the catalytic proton reduction current ( $i_{\text{cat}}/i_p$ ) we find that  $i_{\text{cat}}/i_p$  correlates inversely to TON ( $\text{NH}_3$ ), with  $(\text{C}_6\text{H}_6)_2\text{Cr} > \text{Cp}_2\text{Co} > \text{Cp}^*_2\text{Cr}$  being the order of  $\text{NH}_3$  TON and  $(\text{C}_6\text{H}_6)_2\text{Cr} < \text{Cp}_2\text{Co} < \text{Cp}^*_2\text{Cr}$  being the order of  $i_{\text{cat}}/i_p$ . Interestingly, there is no correlation between  $i_{\text{cat}}/i_p$  and the reduction potential of the different reductants. (C) Proposed mechanism for electrochemical acid reduction, mediated by  $[\text{red}]\text{BAR}^{\text{F}}_4$ , exemplified for  $\text{red} = (\text{C}_6\text{H}_6)_2\text{Cr}$ .

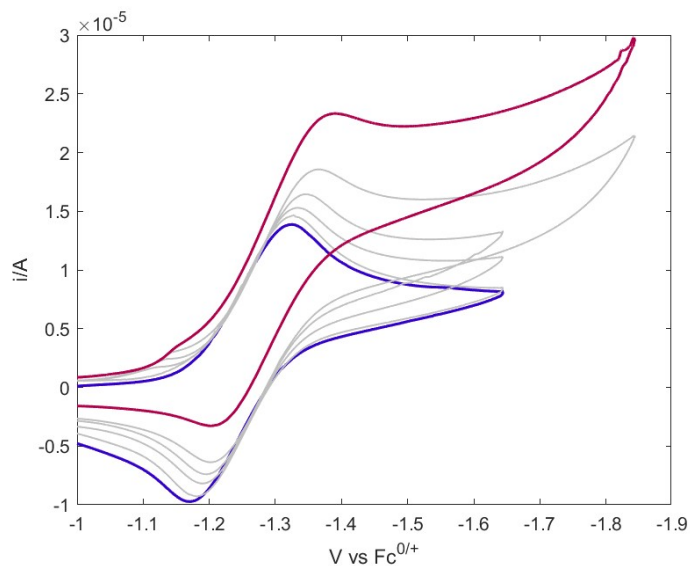


**Figure A.23.** Cyclic voltammograms of  $[(C_6H_6)_2Cr]BArF_4$  (1 mM, dashed lines) in 0.2 M  $[TBA]OTf$ , with increasing  $[Ph_2NH_2]OTf$  added from 0 (blue trace) to 50 equiv (red trace) at  $100 \text{ mV s}^{-1}$  scan rate.

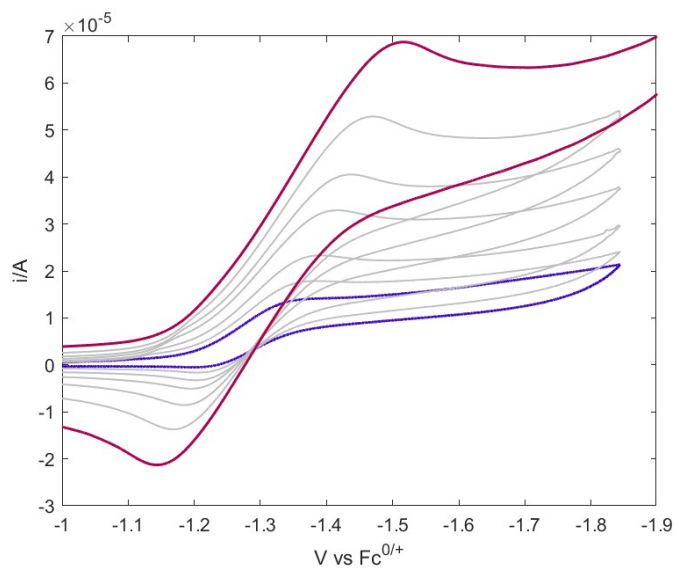


**Figure A.24.** Cyclic voltammograms of  $[(C_6H_6)_2Cr]BArF_4$  (1 mM, dashed lines) in 0.2 M  $[TBA]OTf$ , with 50 equiv  $[Ph_2NH_2]OTf$  added, with varying scan rate from 25 (blue trace) to  $1600 \text{ mV s}^{-1}$  (red trace).

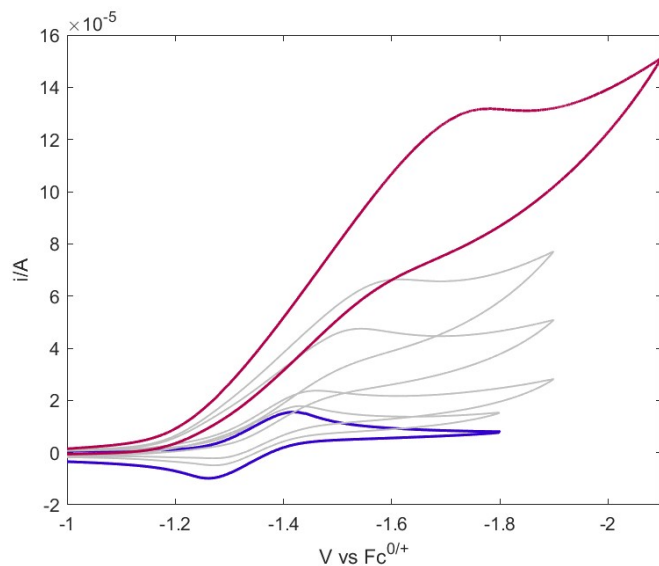


**Figure A.25.** Cyclic voltammograms of  $[\text{Cp}_2\text{Co}]\text{BARF}_4$  (1 mM, dashed lines) in 0.2 M  $[\text{TBA}]\text{OTf}$ , with increasing  $[\text{Ph}_2\text{NH}_2]\text{OTf}$  added from 0 (blue trace) to 50 equiv (red trace) at  $100 \text{ mV s}^{-1}$  scan rate.

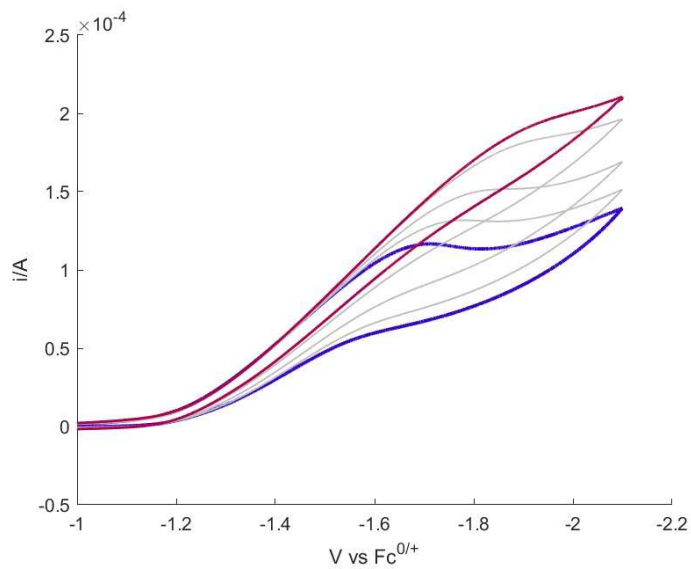


**Figure A.26.** Cyclic voltammograms of  $[\text{Cp}_2\text{Co}]\text{BARF}_4$  (1 mM, dashed lines) in 0.2 M  $[\text{TBA}]\text{OTf}$ , with 50 equiv  $[\text{Ph}_2\text{NH}_2]\text{OTf}$  added, with varying scan rate from 50 (blue trace) to  $800 \text{ mV s}^{-1}$  (red trace).

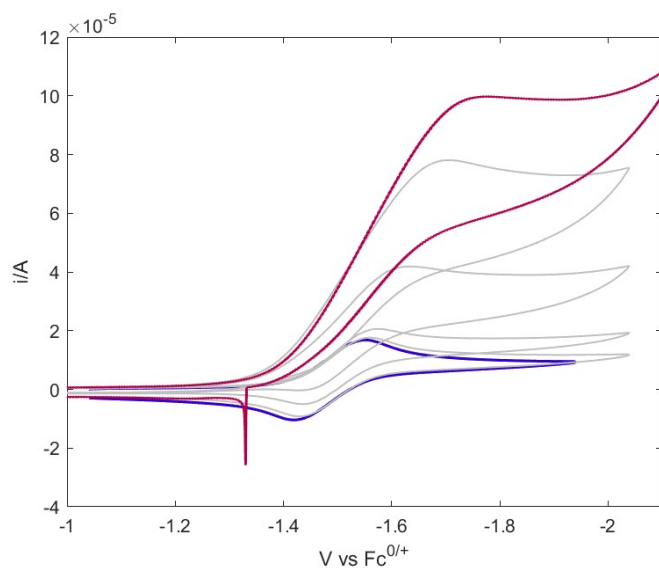


**Figure A.27.** Cyclic voltammograms of  $[\text{Cp}^*_2\text{Cr}]\text{BARF}_4$  (1 mM, dashed lines) in 0.2 M  $[\text{TBA}]\text{OTf}$ , with increasing  $[\text{Ph}_2\text{NH}_2]\text{OTf}$  added from 0 (blue trace) to 50 equiv (red trace) at  $100 \text{ mV s}^{-1}$  scan rate.

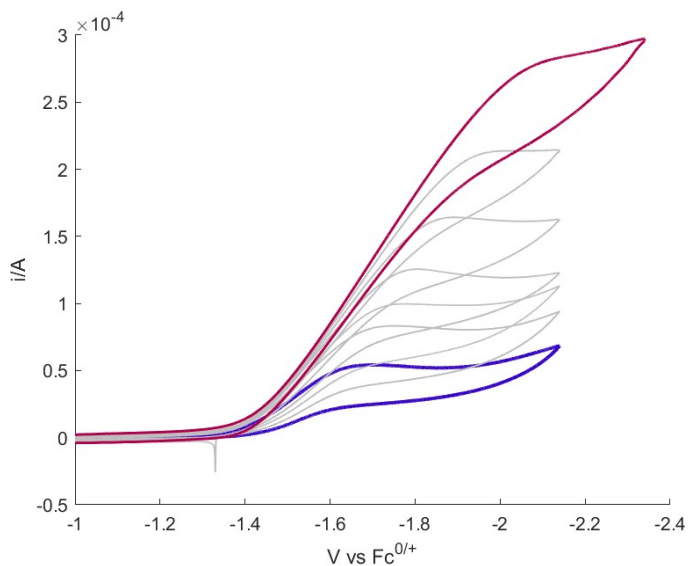


**Figure A.28.** Cyclic voltammograms of  $[\text{Cp}^*_2\text{Cr}]\text{BARF}_4$  (1 mM, dashed lines) in 0.2 M  $[\text{TBA}]\text{OTf}$ , with 50 equiv  $[\text{Ph}_2\text{NH}_2]\text{OTf}$  added, with varying scan rate from 25 (blue trace) to  $1600 \text{ mV s}^{-1}$  (red trace).

### A.8.3 Electrochemical mechanistic studies with [FeCN]

Studies of the electrochemistry of [FeCN] support that catalysis can occur with weak reductants like  $(\text{C}_6\text{H}_6)_2\text{Cr}$ . We have previously measured the reduction potential of  $[\text{FeCN}]^{0/-}$  at  $E_{\text{red}} = -2.07$  V vs.  $\text{Fc}^{+/0}$ ,<sup>1</sup> which is not accessible using  $(\text{C}_6\text{H}_6)_2\text{Cr}$  reductant ( $E_{\text{ox}} = -1.22$  V). Upon addition of  $[\text{Ph}_2\text{NH}_2]\text{OTf}$  to a solution of  $[\text{Fe}^{\text{II}}\text{CN}]$  in THF with 0.2 M  $[\text{TBA}]\text{PF}_6$  electrolyte at 25 °C, we observed that this  $\text{Fe}^{\text{II}}/\text{Fe}^{\text{I}}$  couple shifts to  $E^\circ \approx -1.2$  V (Figure A.29, inset), close to what has been previously observed for  $[\text{FeCNH}]^+[\text{BAr}^{\text{F}}_4]$  ( $E_{\text{red}} = -1.27$  V).<sup>1</sup>

Upon closer inspection, this new reductive couple was composed of two features that partially overlap, with current maxima at  $E_p = -1.15$  V and  $E_p = -1.28$  V (Figure A.29), attributed to  $E([\text{FeCNH}]^{+/0})$  and  $E([\text{FeCNH}_2]^{+/0})$ , respectively. The irreversibility of the first peak ( $E^\circ_{1/2} = -1.10$  V) is attributed to the rapid protonation of electrochemically generated  $[\text{FeCNH}]$ . The second peak ( $E^\circ_{1/2} = -1.23$  V) is irreversible at high acid loadings and slow scan rates (Figure A.30), which is consistent with a multielectron process occurring after the protonation of electrochemically generated  $[\text{FeCNH}_2]$ . Using normalized current  $i_{\text{normalized}} = i/\sqrt{v}$  shows a decrease in current with increasing scan rate, as expected for a catalytic current.

These cyclic voltammetry experiments support our proposed early steps for catalysis. It is worth noting that the measured reduction potential of  $[\text{FeCNH}_2]^{+/0}$  ( $-1.23$  V) would suggest the formation of an equilibrium of these species when  $(\text{C}_6\text{H}_6)_2\text{Cr}$  ( $-1.22$  V) is employed as a reductant, as we observe experimentally (Figure 2.4). Based on this analysis, we cite the  $E^\circ([\text{FeCNH}_2]^{+/0})$  as  $\sim -1.2$  V in the main text. The electrochemical and chemical reactions, as described, are summarized in **Figure A.31**.

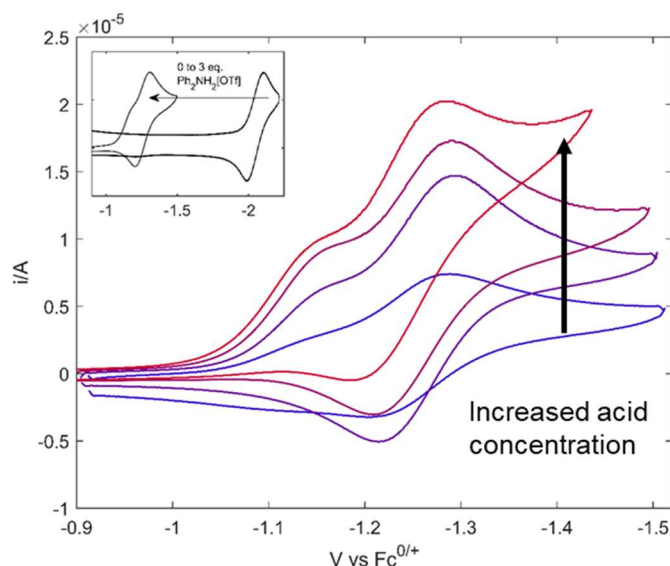


**Figure A.29.** Cyclic voltammograms monitoring the titration of  $[\text{Ph}_2\text{NH}_2]\text{OTf}$  to  $[\text{FeCN}]$ , at  $100 \text{ mV s}^{-1}$  scan rate: 0 to 3 equiv shown in inset, 3 equiv to 20 equiv shown in main figure.

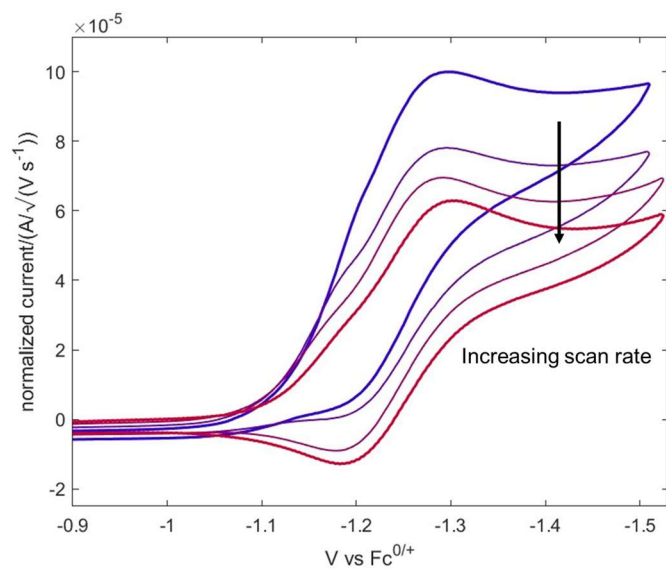


**Figure A.30.** Cyclic voltammograms monitoring scan rate dependence for  $[\text{FeCN}]$  reduction in the presence of 20 equiv  $[\text{Ph}_2\text{NH}_2]\text{OTf}$  from  $10 \text{ mV s}^{-1}$  to  $75 \text{ mV s}^{-1}$ . Normalized current decreases with scan rate as expected for a multielectron process.

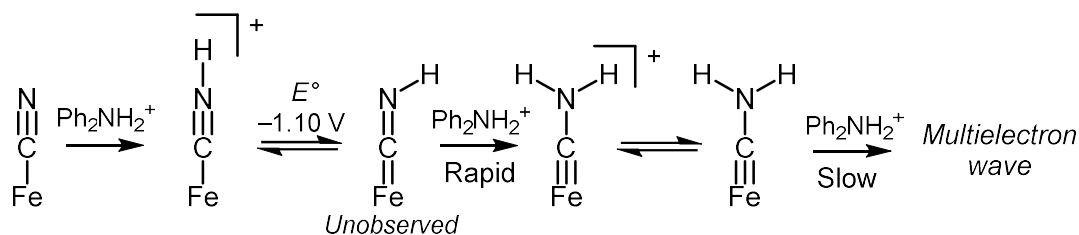


**Figure A.31.** Proposed scheme for cyclic voltammetry measurements.

### A.9. Generation of proposed $[\text{FeC}(\text{H})(\text{NMe}_2)]^+$

For ease of the reader,  $^1\text{H}$ -NMR, UV-vis, and  $^{57}\text{Fe}$  Mössbauer data associated with the synthesis of the proposed carbene species  $[\text{FeC}(\text{H})(\text{NMe}_2)]^+$  are all collated in section A.9, instead of having the individual spectra in the appropriate spectroscopic sections.

#### A.9.1 Generation of UV-vis spectrum of $[\text{FeC}(\text{H})(\text{NMe}_2)]^+$ in the absence of reductant

A cuvette of dilute  $[\text{FeCNMe}_2]^1$  (1 mM) in THF was prepared in the glovebox and sealed with a septum. It was brought out of the glovebox and cooled to  $0^\circ\text{C}$ , with a positive flow of  $\text{N}_2$  supplied with a needle. After equilibration, 5 equiv  $[\text{Ph}_2\text{NH}_2]\text{OTf}$  in 0.25 mL THF were added by syringe, and the reaction was monitored. Within 20 minutes, the initial peak at 420 nm had been consumed with new maxima appearing at 585 nm and 790 nm, as well as a feature that grows beyond the detection limit of the spectrometer (1100 nm). The addition of 10 equiv strong base (TBD) resulted in a loss of these new features and restoration of the initial absorbance at 420 nm, diagnostic for  $[\text{FeCNMe}_2]$ .

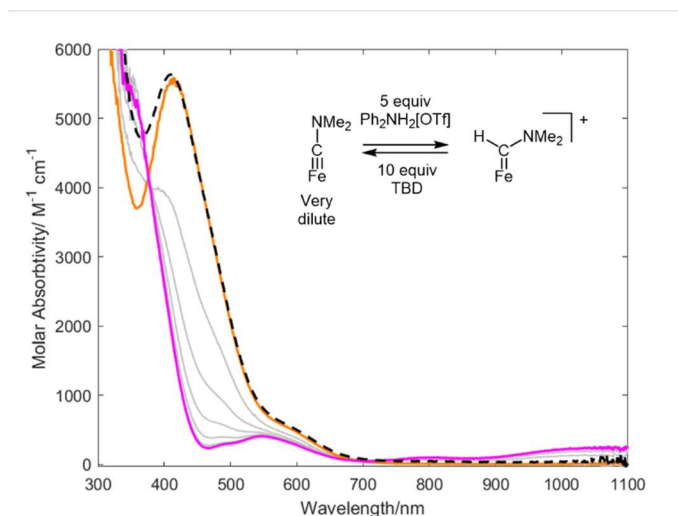


**Figure A.32.** UV-vis monitoring of reaction of  $[\text{FeCNMe}_2]$  (orange trace) and 5 equiv  $[\text{Ph}_2\text{NH}_2]\text{OTf}$  to form  $[\text{FeC}(\text{H})\text{NMe}_2]^+$  (pink trace). 5 minutes between scans, reaction run at  $0^\circ\text{C}$ . The product was monitored to ensure no further reactivity occurred. Excess TBD was added, and the spectrum rapidly regenerated the initially observed spectra of  $[\text{FeCNMe}_2]$  (Black, dashed trace).

### A.9.2 Generation of UV-vis spectrum of $[\text{FeC}(\text{H})(\text{NMe}_2)]^+$ with reductant.

A cuvette of  $[\text{FeCNMe}_2]^1$  (1.5 mM) in THF was prepared in the glovebox and sealed with a septum. It was brought out of the glovebox with a positive flow of  $\text{N}_2$  supplied with a needle during UV-vis monitoring. The cuvette was cooled to  $-20^\circ\text{C}$ , and after equilibration (10 min), 10 equiv  $[\text{Ph}_2\text{NH}_2]\text{OTf}$  in 0.25 mL THF was added via syringe, followed by 10 equiv  $(\text{C}_6\text{H}_6)_2\text{Cr}$  in 0.5 mL THF (also added by syringe). The reaction was monitored, with the absorption maxima at 420 nm associated with  $[\text{FeCNMe}_2]$  consumed with and new maxima growing in at 790 nm, as well as a feature that grows beyond the detection limit of the spectrometer (1100 nm). These new maxima matched the spectra for the proposed  $[\text{FeC}(\text{H})(\text{NMe}_2)]^+$  formed from the reaction of  $[\text{FeCNMe}_2]$  with  $[\text{Ph}_2\text{NH}_2]\text{OTf}$  (Figure A.32). High energy transitions were obscured by  $(\text{C}_6\text{H}_6)_2\text{Cr}^{0/+}$ .

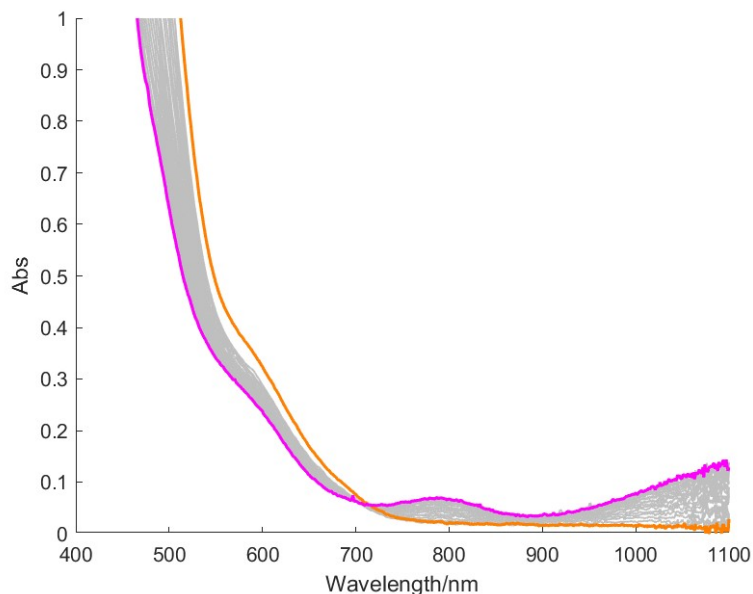


**Figure A.33.** UV-vis monitoring of reaction of  $[\text{FeCNMe}_2]$  (pink trace) and with 10 equiv  $[\text{Ph}_2\text{NH}_2]\text{OTf}$  and 10 equiv  $(\text{C}_6\text{H}_6)_2\text{Cr}$  to form  $[\text{FeC}(\text{H})\text{NMe}_2]^+$  (pink trace) at room temperature. 30 seconds between scans.

### A.9.3 $[\text{FeC}(\text{H})(\text{NMe}_2)]^+$ generation for NMR experiments

A J. Young NMR tube was loaded with  $[\text{FeCNMe}_2]$  (5 mM) in  $d_8$ -THF (0.5 mL) in the glovebox.  $[\text{Ph}_2\text{NH}_2]\text{OTf}$  (25  $\mu\text{mol}$ , 10 equiv) was added as a solid, and  $^1\text{H}$  NMR was collected. The formation of  $[\text{FeCNMe}_2]^+$ ,  $\text{H}_2$  and a new species were observed. Characteristic peaks (that do not overlap with acid or  $[\text{FeCNMe}_2]^+$ ), for this new species were at 23.4 ppm, 5.08 ppm, -2.00 ppm. Addition of  $(\text{C}_6\text{H}_6)_2\text{Cr}$  (25  $\mu\text{mol}$ , 10 equiv) resulted in complete consumption of  $[\text{FeCNMe}_2]^+$  and an increase concentration of the new species. Over time, this species decays to form  $[\text{FeOTf}]$ . After one week,  $[\text{FeOTf}]$  was the only major paramagnetic Fe-species left. The contents of the tube were cooled to  $-78^\circ\text{C}$  and transferred to a Schlenk flask, which was subsequently frozen to 77 K. Once frozen, the flask was opened to air, and  $\text{KO}^t\text{Bu}$  was added as a solid. The volatiles were vacuum transferred onto a receiving flask of 3 ml 1 M HCl in  $\text{Et}_2\text{O}$ . The receiving flask was thawed, and solvent was removed *in vacuo* to leave a solid precipitate. This was taken up in  $d_6$ -DMSO with a known amount of 1,3,5-trimethoxybenzene added, with  $[\text{Me}_2\text{NH}_2]\text{Cl}$  and  $[\text{Me}_3\text{NH}]\text{Cl}$  both detectable as volatile basic products (Figure A.36).

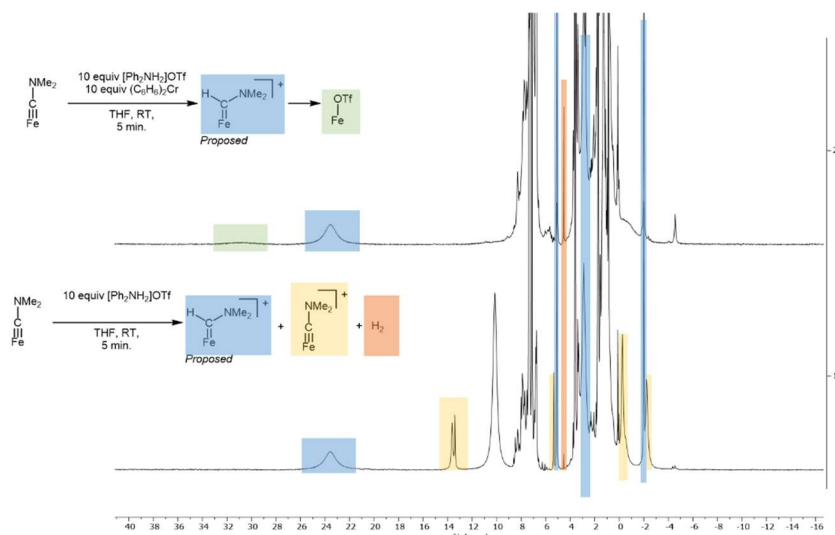


**Figure A.34.** <sup>1</sup>H NMR spectra of reaction of  $P_3SiFeCNMe_2$  with 10 equiv  $[Ph_2NH_2]OTf$  (top) and reaction of  $P_3SiFeCNMe_2$  with 10 equiv  $[Ph_2NH_2]OTf$  and 10 equiv  $(C_6H_6)_2Cr$  (bottom). Peaks diagnostic for  $[FeC(H)NMe_2]^+$ ,  $[Fe(OTf)]$ ,  $H_2$ , and the proposed  $[FeC(H)NMe_2]^+$  are highlighted.

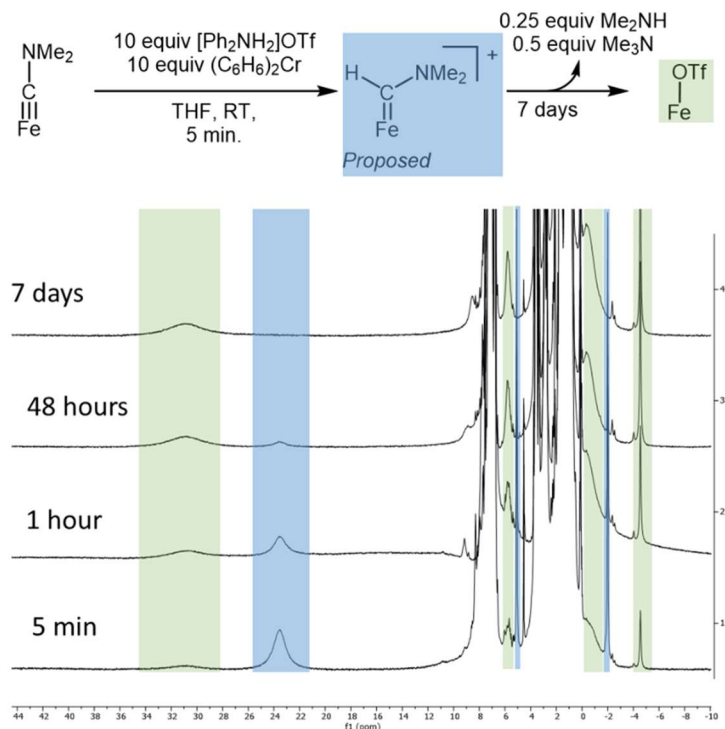


**Figure A.35.** Reaction of  $P_3SiFeCNMe_2$  with 10 equiv  $[Ph_2NH_2]OTf$  and 10 equiv  $(C_6H_6)_2Cr$  (bottom), monitored overtime. Peaks diagnostic for  $[Fe(OTf)]$  and the proposed  $[FeC(H)NMe_2]^+$  are highlighted.

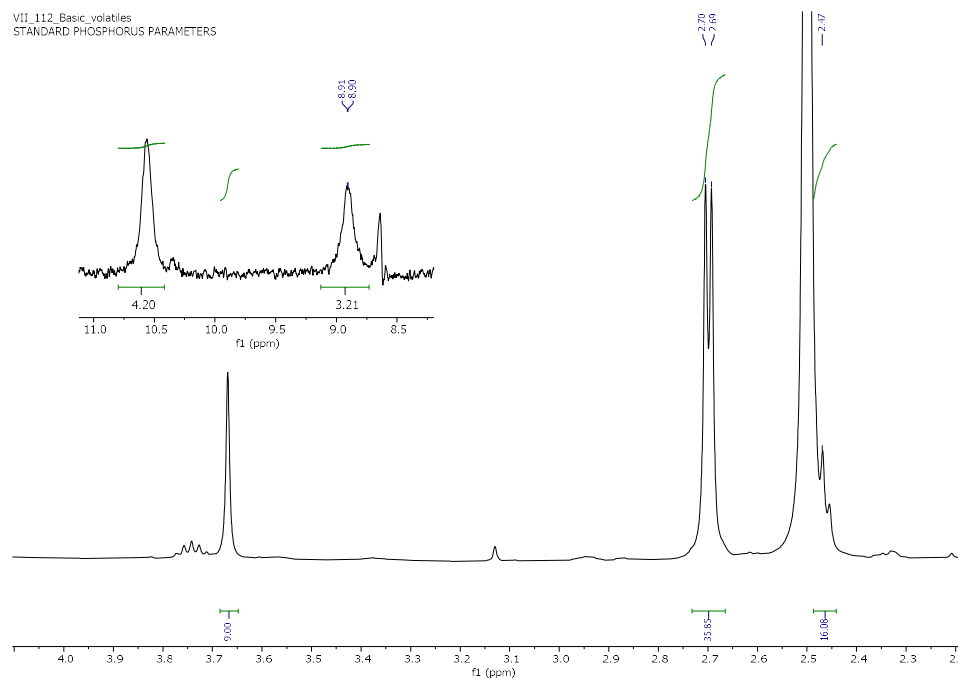
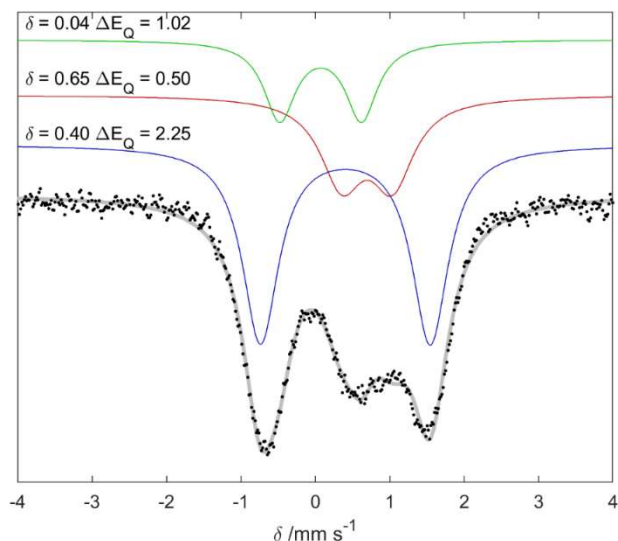


**Figure A.36.** Volatile basic products from the reaction of  $P_3^{Si}FeCNMe_2$  with 10 equiv  $[Ph_2NH_2]OTf$  and 10 equiv  $(C_6H_6)_2Cr$ , with  $[Me_2NH_2]Cl$  ( $\delta$  8.8, br, 2H,  $\delta$  2.48, t,  $J = 6$  Hz, 6H) and  $[Me_3NH]Cl$  ( $\delta$  10.6, br, 2H,  $\delta$  2.69, d,  $J = 5.2$  Hz, 9H) products.

#### A.9.4 Mössbauer experiment

The Mössbauer spectrum of this proposed carbene species ( $[FeC(H)(NMe_2)]^+$ ) was generated by reacting  $[FeCNMe_2]$  (25 mg, 35  $\mu$ mol) with 10 equiv  $(C_6H_6)_2Cr$  (72 mg, 350  $\mu$ mol) and 10 equiv  $[Ph_2NH_2]OTf$  (95 mg, 350  $\mu$ mol) in 0.8 mL THF at room temperature for 5 minutes. The reaction was transferred to a Mössbauer cup and frozen at 77 K.



Trace	$\delta$ (mm s <sup>-1</sup> )	$\Delta E_Q$ (mm s <sup>-1</sup> )	Relative area	Assignment
Blue	0.40±0.01	2.25±0.01	54 %	[FeC(H)(NMe <sub>2</sub> )] <sup>+</sup>
Red	0.65±0.05	0.5±0.1	26%	[FeOTf]
Green	0.04±0.05	1.02±0.1	19 %	[FeCNMe <sub>2</sub> ]

**Figure A.37.** Mössbauer spectrum of reaction of P<sub>3</sub><sup>Si</sup>FeCNMe<sub>2</sub> with 10 equiv each of (C<sub>6</sub>H<sub>6</sub>)<sub>2</sub>Cr and [Ph<sub>2</sub>NH<sub>2</sub>]OTf. The major species (blue) is proposed to be [FeC(H)(NMe<sub>2</sub>)]<sup>+</sup>, with the other species matching previously characterized [FeOTf]<sup>10</sup> and [FeCNMe<sub>2</sub>].<sup>1</sup>

#### A.10 Derivation of estimated BDFE for early N–H bonds

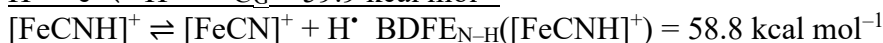
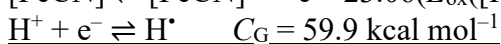
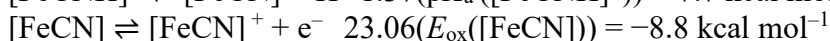
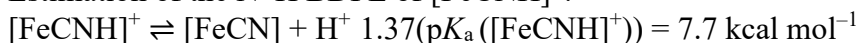
To derive the early N–H bond Bond Dissociation Free Energies (BDFE), we have used previously measured values,<sup>10</sup> but with updated  $C_G$  constants, which have, since our initial publication, been measured in THF ( $C_G = 59.9$  kcal mol<sup>-1</sup>),<sup>12</sup> allowing us to derive BDFEs and not only BDEs. For clarity, the thermochemical parameters previously measured are presented again in Table A.5. The BDFEs are derived using these values.

In addition, we derive the BDFE<sub>eff</sub> for the combination of (C<sub>6</sub>H<sub>6</sub>)<sub>2</sub>Cr/[Ph<sub>2</sub>NH<sub>2</sub>]OTf used as a reference for the  $\Delta G$  derived for H<sup>+</sup>/e<sup>-</sup> addition in Figure 2.7 in the main text.

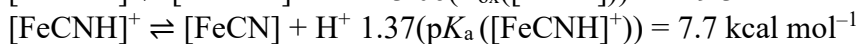
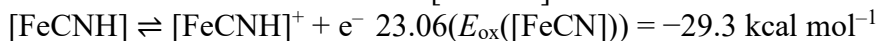
**Table A.5.**  $E_{\text{ox}}$  and  $\text{p}K_{\text{a}}$  for  $[\text{FeCNH}_x]$  species and  $(\text{C}_6\text{H}_6)_2\text{Cr}$  and  $[\text{Ph}_2\text{NH}_2]\text{OTf}$  used to derive  $\text{BDFE}_{\text{N-H}}$  and  $\text{BDFE}_{\text{eff}}$ .

Compound	$E_{\text{ox}}$ (vs. $\text{Fc}^{+/0}$ in THF)	$\text{p}K_{\text{a}}$ (in THF)
$[\text{FeCN}]$	-0.38 V	
$[\text{FeCNH}]^+$	-0.17 V	5.6
$[\text{FeCNH}]$	-1.27 V	
$[\text{FeCN}(\text{Me})\text{H}]^+$		7.1
$[\text{FeCN}(\text{Me})\text{H}]$	-1.27 V	
$[\text{FeCNMe}]$	-1.31 V	
$(\text{C}_6\text{H}_6)_2\text{Cr}$	-1.22 V	
$[\text{Ph}_2\text{NH}_2]\text{OTf}$		3.2

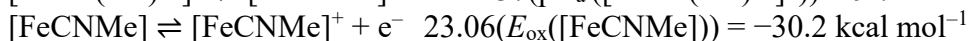
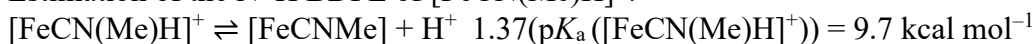
Estimation of the N–H BDFE of  $[\text{FeCNH}]^+$ :



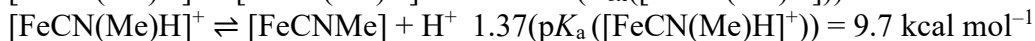
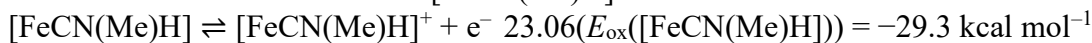
Estimation of the N–H BDFE of  $[\text{FeCNH}]$ :



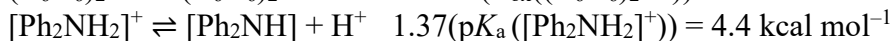
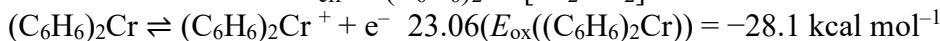
Estimation of the N–H BDFE of  $[\text{FeCN}(\text{Me})\text{H}]^+$ :



Estimation of the N–H BDFE of  $[\text{FeCN}(\text{Me})\text{H}]$ :



Estimation of the  $\text{BDFE}_{\text{eff}}$  of  $(\text{C}_6\text{H}_6)_2\text{Cr}/[\text{Ph}_2\text{NH}_2]\text{OTf}$ :



## A.11 Computational Methods

### A.11.1 General overview of computational details

As stated in the main text for our computational studies, we employed the TPSS functional<sup>13</sup> and a def2-TZVP basis set on transition metals and a def2-SVP basis set on all other atoms,<sup>14</sup> which we have previously demonstrated accurately replicate BDFEs on similar platforms.<sup>15</sup> The ORCA open-source software package was used.<sup>16</sup>

The numerical frequencies of the minimized structures were calculated to ensure that these structures represented local minima and not saddle points. Entropic and internal energy contributions were calculated at 195 K, 253 K, 273 K, and 293 K to compute the  $\Delta G_f$  at these temperatures.

For the analysis in Figure 2.6, a comparison of the lowest energy isomers is presented in Tables A.6, A.7, and A.8. Key bond lengths and their comparison to relevant crystallographic data are presented in Table A.9. For the analysis in Figure 2.7, the energy of each pathway is presented in Figures A.38 and A.39. The final step(s) to convert the final intermediate in pathways *i-iii* (as defined in Figure 2.7) to an on-path species  $[\text{FeCNH}]^{+/0}$  is presented in Figure A.39. The calculations to derive the  $\Delta G$  in Figure 2.7 and Figure A.38, A.39 are summarized in Tables A.10-A.14.

### A.11.2 Treatment of H<sup>+</sup>

The treatment of  $S(\text{H}^+)$  in calculations can be a source of systematic error in DFT calculations, therefore it is useful to detail how this value has been derived. We have taken an *ab initio* approach to  $S(\text{H}^+)$  using the !PRINTTHERMOCHEM function in ORCA 5.0<sup>17</sup> to calculate the translational entropy and internal energy of H<sup>+</sup> at temperatures 195 K, 253 K, 273 K, and 293 K. These values are used directly to derive the  $\Delta G_f(\text{H}^+)$  values as presented in Table A.9.

### A.11.3 Calculating $\Delta G$ for bond formations in Figure 2.7

In the analysis of step g in Figure 2.7, we use the computations presented in Figures A.38-A.39 and Tables A.10-A.14 to guide the discussion. However, for clarity for bond formation steps, we reference these H-atom transfers from the addition of H<sup>+</sup> from

[Ph<sub>2</sub>NH<sub>2</sub>]OTf and e<sup>-</sup> from (C<sub>6</sub>H<sub>6</sub>)<sub>2</sub>Cr to the BDFE<sub>eff</sub> of this reagent combination, derived in section A.10 to be 36.2 kcal mol<sup>-1</sup>.

For example, for the addition of an H-atom to [FeC(H)(NH<sub>2</sub>)]<sup>+</sup> to [FeC(H)(NH<sub>3</sub>)]<sup>+</sup>, the BDFE<sub>N-H</sub> of this bond is 14 kcal mol<sup>-1</sup> (Table A.11). The ΔG, as reported in Figure 2.7 and Figures A.38-A.39, is then given as ΔG = BDFE<sub>eff</sub> - BDFE<sub>N-H</sub> = 36-14 = +22 kcal mol<sup>-1</sup>.

**Table A1.6.** Table of experimental<sup>10</sup> and computationally derived bond dissociation free energies and comparison to relevant experimental values.

	BDFE <sub>195K</sub> (kcal mol <sup>-1</sup> )	BDFE <sub>253K</sub> (kcal mol <sup>-1</sup> )	BDFE <sub>273K</sub> (kcal mol <sup>-1</sup> )	BDFE <sub>298K</sub> (kcal mol <sup>-1</sup> )	BDFE <sub>298 K, exp</sub> (kcal mol <sup>-1</sup> )
P <sub>3</sub> <sup>Si</sup> FeCNH <sub>2</sub> <sup>+</sup> → P <sub>3</sub> <sup>Si</sup> FeCNH <sup>+</sup> +H <sup>•</sup>	42	40	39	38	
P <sub>3</sub> <sup>Si</sup> FeCHNH <sub>2</sub> <sup>+</sup> → P <sub>3</sub> <sup>Si</sup> FeCNH <sub>2</sub> <sup>+</sup> +H <sup>•</sup>	55	53	53	52	
P <sub>3</sub> <sup>Si</sup> FeCHNH <sub>2</sub> → P <sub>3</sub> <sup>Si</sup> FeCNH <sub>2</sub> +H <sup>•</sup>	49	48	47	47	
P <sub>3</sub> <sup>Si</sup> FeCNH <sub>2</sub> → P <sub>3</sub> <sup>Si</sup> FeCNH +H <sup>•</sup>	38	36	35	35	
<hr/>					
P <sub>3</sub> <sup>Si</sup> FeCN(Me)H <sup>+</sup> → P <sub>3</sub> <sup>Si</sup> FeCNMe <sup>+</sup> +H <sup>•</sup>					41
P <sub>3</sub> <sup>Si</sup> FeCN(Me)H → P <sub>3</sub> <sup>Si</sup> FeCNMe +H <sup>•</sup>					40

**Table A.7.** Computationally derived free energies of intermediates of (P<sub>3</sub><sup>Si</sup>FeCNH<sub>2</sub> + H<sup>•</sup>).

Compound	Spin state	ΔG <sub>f,195</sub> (Eh)	ΔG <sub>f,253</sub> (Eh)	ΔG <sub>f,273</sub> (Eh)	ΔG <sub>f,298</sub> (Eh)	ΔG <sub>rel,195</sub> (kcal mol <sup>-1</sup> )	ΔG <sub>rel,253</sub> (kcal mol <sup>-1</sup> )	ΔG <sub>rel,273</sub> (kcal mol <sup>-1</sup> )	ΔG <sub>rel,298</sub> (kcal mol <sup>-1</sup> )
<b>P<sub>3</sub><sup>Si</sup>Fe(CNH<sub>3</sub>)<sup>+</sup> species</b>									
P <sub>3</sub> <sup>Si</sup> FeC(H)(NH <sub>2</sub> ) <sup>+</sup>	triplet	-4076.57	-4076.59	-4076.59	-4076.60	0.0	0.0	0.0	0.0
P <sub>3</sub> <sup>Si</sup> FeC(H)(NH <sub>2</sub> ) <sup>+</sup>	singlet	-4076.55	-4076.57	-4076.58	-4076.59	9.3	9.5	9.6	9.7
P <sub>3</sub> <sup>Si</sup> FeC(H)(NH <sub>2</sub> ) <sup>+</sup>	quintet	-4076.51	-4076.53	-4076.53	-4076.54	39.1	38.7	38.6	38.4
P <sub>3</sub> <sup>Si</sup> FeCNH <sub>3</sub> <sup>+</sup>	singlet	-4076.50	-4076.51	-4076.52	-4076.53	45.1	45.6	45.7	46.0
P <sub>3</sub> <sup>Si</sup> FeCNH <sub>3</sub> <sup>+</sup>	triplet	-4076.46	-4076.48	-4076.49	-4076.50	65.5	65.7	65.8	65.9
P <sub>3</sub> <sup>Si</sup> Fe(H)CNH <sub>2</sub> <sup>+</sup>	singlet	-4076.56	-4076.57	-4076.58	-4076.59	6.9	7.7	7.8	8.0
P <sub>3</sub> <sup>Si</sup> FeC <sup>+</sup>	singlet	-4019.92	-4019.94	-4019.94	-4019.95	-	-	-	-
P <sub>3</sub> <sup>Si</sup> FeC <sup>+</sup> +NH <sub>3</sub>	singlet	-4076.48	-4076.51	-4076.51	-4076.52	53.3	51.2	50.5	49.6
<b>P<sub>3</sub><sup>Si</sup>Fe(CNH<sub>3</sub>) species</b>									
P <sub>3</sub> <sup>Si</sup> FeC(H)(NH <sub>2</sub> )	doublet	-4076.73	-4076.75	-4076.75	-4076.76	0.0	0.0	0.0	0.0
P <sub>3</sub> <sup>Si</sup> FeC(H)(NH <sub>2</sub> )	quartet	-4076.68	-4076.70	-4076.71	-4076.72	28.6	28.4	28.4	28.3
P <sub>3</sub> <sup>Si</sup> FeCNH <sub>3</sub>	doublet	-4076.62	-4076.64	-4076.65	-4076.66	66.1	66.0	66.0	65.9
P <sub>3</sub> <sup>Si</sup> Fe(H)CNH <sub>2</sub>	doublet	-4076.70	-4076.72	-4076.72	-4076.73	18.5	19.1	19.1	19.0
P <sub>3</sub> <sup>Si</sup> FeC	doublet	-4020.10	-4020.12	-4020.13	-4020.14	-	-	-	-
P <sub>3</sub> <sup>Si</sup> FeC + NH <sub>3</sub>	doublet	-4076.67	-4076.69	-4076.70	-4076.71	39.2	36.9	36.0	35.0

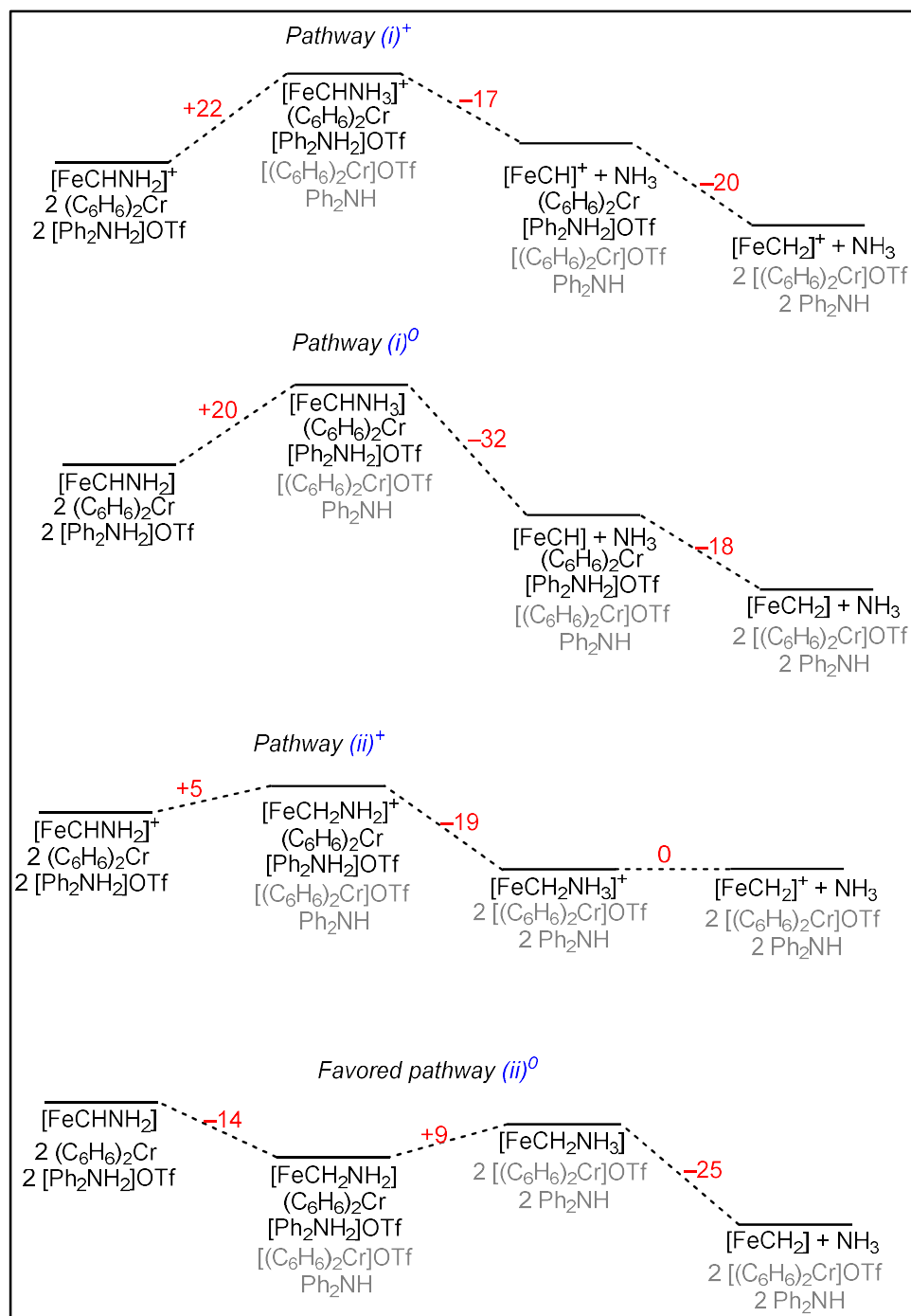
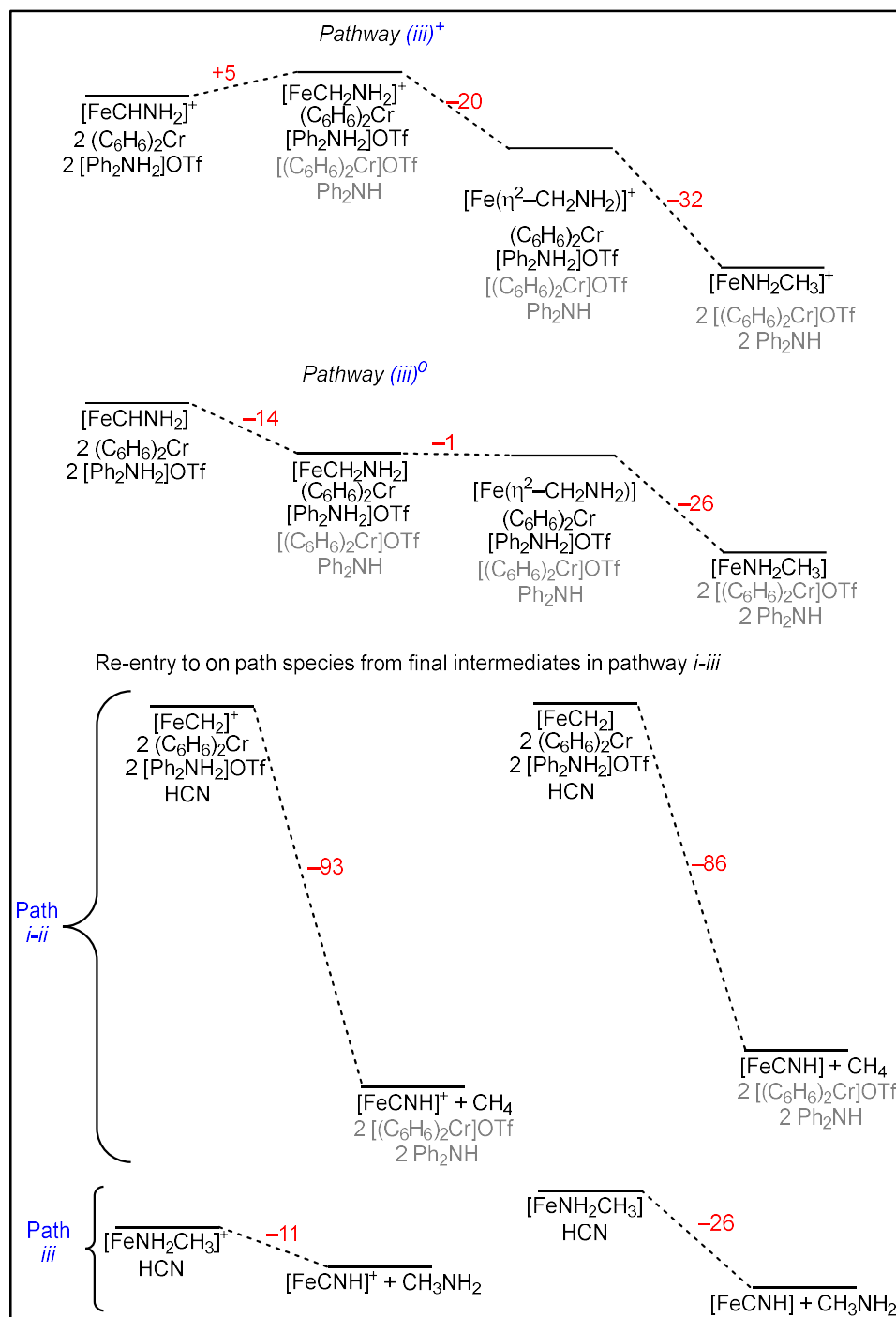


Figure A.38. Thermodynamic barriers for CH<sub>4</sub> and NH<sub>3</sub> selective pathways *i-ii*.



**Figure A.39.** Thermodynamic barriers for  $\text{CH}_3\text{NH}_2$  selective pathways *iii* and thermodynamic barriers for release of substrate, and rebinding of  $\text{CN}^-$ .

**Table A.18.** Computationally derived free energies of early intermediates of  $P_3^{Si}FeCN$  reduction.

Compound	Spin state	$\Delta G_{f,195}$ (Eh)	$\Delta G_{f,253}$ (Eh)	$\Delta G_{f,273}$ (Eh)	$\Delta G_{f,298}$ (Eh)
$P_3^{Si}FeCNH^+$	triplet	-4075.40	-4075.42	-4075.43	-4075.44
$P_3^{Si}FeCNH$	doublet	-4075.58	-4075.60	-4075.60	-4075.61
$P_3^{Si}FeCNH_2^+$	doublet	-4075.98	-4075.99	-4076.00	-4076.01
$P_3^{Si}FeCNH_2$	singlet	-4076.14	-4076.16	-4076.17	-4076.18

**Table A.9.** Experimentally<sup>1,8,10</sup> and computationally derived key bond lengths and comparison with known crystallographic data.

In general, the Fe–P and Fe–Si bonds are very reliably reproduced computationally. Increased error is observed in the C–N bond. This is likely partially attributable to the use of methylated analogs (due to the instability of the compounds) and the hydrogen bonds formed to N–H in  $P_3^{Si}FeCNH^+$  and  $P_3^{Si}FeCNH_2^+$ . The Fe–C bond length is consistently overestimated by about 0.05 Å by DFT.

Compound		C–N (Å)	Fe–C (Å)	Fe–P <sub>ave</sub> (Å)	Fe–Si (Å)	<Fe–C–N
$P_3^{Si}FeCNH^+$	Computed	1.186	1.857	2.368	2.331	177.1
$P_3^{Si}FeCNH^+$	Crystal.	1.144	1.913	2.384	2.305	178.4
$P_3^{Si}FeCNH$	Computed	1.228	1.774	2.266	2.289	175.6
$P_3^{Si}FeCNMe$	Crystal	1.186	1.821	2.273	2.273	177.6
$P_3^{Si}FeCNH_2^+$	Computed	1.317	1.684	2.316	2.358	176.5
$P_3^{Si}FeCNH_2^+$	Crystal	1.223	1.799	2.314	2.311	174.2
$P_3^{Si}FeCNMe_2^+$	Crystal	1.310	1.736	2.364	2.358	173.8
$P_3^{Si}FeCNH_2$	Computed	1.337	1.675	2.214	2.310	179.1
$P_3^{Si}FeCNMe_2$	Crystal	1.328	1.710	2.230	2.305	177.8
$P_3^{Si}FeCH^+$	Computed	-	1.65	2.30	2.38	-
$P_3^{Si}FeCMe^+$	Crystal	-	1.70	2.34	2.39	-
$P_3^{Si}FeCH$	Computed	-	1.65	2.21	2.32	-
$P_3^{Si}FeCMe$	Crystal	-	1.67	2.25	2.33	-

**Table A.10.** Computationally derived energies of small molecules relevant to calculations.

Compound	Spin state	$\Delta G_{f,195}$ (Eh)	$\Delta G_{f,253}$ (Eh)	$\Delta G_{f,273}$ (Eh)	$\Delta G_{f,298}$ (Eh)
HCN	singlet	-93.47	-93.48	-93.48	-93.48
MeNH <sub>2</sub>	singlet	-95.86	-95.87	-95.87	-95.87
CH <sub>4</sub>	singlet	-40.51	-40.51	-40.51	-40.51
NH <sub>3</sub>	singlet	-56.57	-56.57	-56.57	-56.57
H•	doublet	-0.5062	-0.5086	-0.5094	-0.5105

**Table A.11.** Table of computationally derived energies of isomers and spin states of P<sub>3</sub><sup>Si</sup>Fe(CNH<sub>4</sub>). Values derived here are used in Figures 2.7, A.37, and A.38.

Compound	Spin state	$\Delta G_{f,195}$ (Eh)	$\Delta G_{f,253}$ (Eh)	$\Delta G_{f,273}$ (Eh)	$\Delta G_{f,298}$ (Eh)	$\Delta G_{rel,195}$ (kcal mol <sup>-1</sup> )	$\Delta G_{rel,253}$ (kcal mol <sup>-1</sup> )	$\Delta G_{rel,273}$ (kcal mol <sup>-1</sup> )	$\Delta G_{rel,298}$ (kcal mol <sup>-1</sup> )
P <sub>3</sub> <sup>Si</sup> FeCHNH <sub>2</sub> <sup>+</sup> + H•	-	-4077.07	-4077.10	-4077.10	-4077.11	0	0	0	0
P <sub>3</sub> <sup>Si</sup> FeCHNH <sub>3</sub> <sup>+</sup>	doublet	-4077.10	-4077.12	-4077.13	-4077.14	-17	-15	-14	-14
P <sub>3</sub> <sup>Si</sup> FeCH <sup>+</sup>	doublet	-4020.55	-4020.57	-4020.58	-4020.59	-	-	-	-
P <sub>3</sub> <sup>Si</sup> FeCH <sup>+</sup> + NH <sub>3</sub>	doublet	-4077.12	-4077.14	-4077.15	-4077.16	-29	-30	-30	-30
P <sub>3</sub> <sup>Si</sup> FeCH <sub>2</sub> NH <sub>2</sub> <sup>+</sup>	quartet	-4077.13	-4077.15	-4077.15	-4077.16	-34	-32	-32	-31
P <sub>3</sub> <sup>Si</sup> Fe( $\eta^2$ -CH <sub>2</sub> NH <sub>2</sub> ) <sup>+</sup>	doublet	-4077.16	-4077.18	-4077.19	-4077.20	-54	-52	-52	-51

**Table A.12.** Table of computationally derived energies of isomers and spin states of P<sub>3</sub><sup>Si</sup>Fe(CNH<sub>4</sub>). Values derived here are used in Figures 2.7, A.37, and A.38.

Compound	Spin state	$\Delta G_{f,195}$ (Eh)	$\Delta G_{f,253}$ (Eh)	$\Delta G_{f,273}$ (Eh)	$\Delta G_{f,298}$ (Eh)	$\Delta G_{rel,195}$ (kcal mol <sup>-1</sup> )	$\Delta G_{rel,253}$ (kcal mol <sup>-1</sup> )	$\Delta G_{rel,273}$ (kcal mol <sup>-1</sup> )	$\Delta G_{rel,298}$ (kcal mol <sup>-1</sup> )
P <sub>3</sub> <sup>Si</sup> FeCHNH <sub>2</sub> + H•	-	-4077.24	-4077.26	-4077.26	-4077.27	0	0	0	0
P <sub>3</sub> <sup>Si</sup> FeCHNH <sub>3</sub> constrained	singlet	-4077.26	-4077.28	-4077.29	-4077.30	-17	-17	-16	-16
P <sub>3</sub> <sup>Si</sup> FeCH	singlet	-4020.74	-4020.76	-4020.77	-4020.78	-	-	-	-
P <sub>3</sub> <sup>Si</sup> FeCH + NH <sub>3</sub>	singlet	-4077.31	-4077.33	-4077.34	-4077.35	-47	-48	-48	-48
P <sub>3</sub> <sup>Si</sup> FeCH <sub>2</sub> NH <sub>2</sub>	triplet	-4077.32	-4077.34	-4077.34	-4077.35	-52	-51	-50	-50
P <sub>3</sub> <sup>Si</sup> Fe( $\eta^2$ -CH <sub>2</sub> NH <sub>2</sub> )	singlet	-4077.32	-4077.34	-4077.35	-4077.36	-54	-52	-52	-51

**Table A.13.** Table of computationally derived energies of isomers and spin states of  $P_3^{Si}Fe(CNH_5)^+$ . Values derived here are used in Figures 2.7, A.37, and A.38.

Compound	Spin state	$\Delta G_{f,195}$ (Eh)	$\Delta G_{f,253}$ (Eh)	$\Delta G_{f,273}$ (Eh)	$\Delta G_{f,298}$ (Eh)	$\Delta G_{rel,195}$ (kcal mol <sup>-1</sup> )	$\Delta G_{rel,253}$ (kcal mol <sup>-1</sup> )	$\Delta G_{rel,273}$ (kcal mol <sup>-1</sup> )	$\Delta G_{rel,298}$ (kcal mol <sup>-1</sup> )
$P_3^{Si}Fe(\eta^2-CH_2NH_2)^+ + H.$		-4077.67	-4077.69	-4077.70	-4077.71	0	0	0	0
$P_3^{Si}FeCH_2NH_3^+$	triplet	-4077.73	-4077.75	-4077.75	-4077.76	-37	-36	-36	-35
$P_3^{Si}FeCH_2^+$	triplet	-4021.16	-4021.17	-4021.18	-4021.19	-	-	-	-
$P_3^{Si}FeCH_2^+$	singlet	-4021.15	-4021.17	-4021.18	-4021.19	-	-	-	-
$P_3^{Si}FeCH_2^+ + NH_3$	triplet	-4077.72	-4077.74	-4077.75	-4077.76	-34	-35	-35	-36
$P_3^{Si}FeNH_2CH_3^+$	triplet	-4077.78	-4077.80	-4077.80	-4077.81	-70	-69	-68	-68

**Table A.14.** Table of computationally derived energies of isomers and spin states of  $P_3^{Si}Fe(CNH_5)$ . Values derived here are used in Figures 2.7, A.37, and A.38.

Compound	Spin state	$\Delta G_{f,195}$ (Eh)	$\Delta G_{f,253}$ (Eh)	$\Delta G_{f,273}$ (Eh)	$\Delta G_{f,298}$ (Eh)	$\Delta G_{rel,195}$ (kcal mol <sup>-1</sup> )	$\Delta G_{rel,253}$ (kcal mol <sup>-1</sup> )	$\Delta G_{rel,273}$ (kcal mol <sup>-1</sup> )	$\Delta G_{rel,298}$ (kcal mol <sup>-1</sup> )
$P_3^{Si}Fe(\eta^2-CH_2NH_2) + H.$		-4077.83	-4077.85	-4077.86	-4077.87	0	0	0	0
$P_3^{Si}FeCH_2NH_3$	doublet	-4077.87	-4077.89	-4077.90	-4077.91	-28	-27	-27	-26
$P_3^{Si}FeCH_2$	doublet	-4021.34	-4021.36	-4021.37	-4021.38	-	-	-	-
$P_3^{Si}FeCH_2 + NH_3$	doublet	-4077.91	-4077.93	-4077.94	-4077.95	-50	-51	-51	-52
$P_3^{Si}FeNH_2CH_3$	doublet	-4077.93	-4077.95	-4077.96	-4077.97	-64	-63	-63	-62

## A.12 References for Appendix A

1. Rittle, J.; Peters, J. C. *Angew. Chem. Int. Ed.* **2016**, 55, 12262–12265.
2. Anderson, J. S.; Moret, M.-E.; Peters, J. C. *J. Am. Chem. Soc.* **2013**, 135, 534–537.
3. Betley, T. A.; Peters, J. C. *J. Am. Chem. Soc.* **2004**, 126, 6252–6254.
4. Chalkley, M. J.; Del Castillo, T. J.; Matson, B. D.; Roddy, J. P.; Peters, J. C. *ACS Cent. Sci.* **2017**, 3, 217–223. .
5. Del Castillo, T. J.; Thompson, N. B.; Peters, J. C. *J. Am. Chem. Soc.* **2016**, 138, 5341–5350.
6. Erhardt, S.; Grushin, V. V.; Kilpatrick, A. H.; Macgregor, S. A.; Marshall, W. J.; Roe, D. C. *J. Am. Chem. Soc.* **2008**, 130, 4828–4845.
7. Fulmer, G. R.; Miller, A. J. M.; Sherden, N. H.; Gottlieb, H. E.; Nudelman, A.; Stoltz, B. M.; Bercaw, J. E.; Goldberg, K. I. *Organometallics* **2010**, 29, 2176–2179.

8. Citek, C.; Oyala, P. H.; Peters, J. C. *J. Am. Chem. Soc.* **2019**, 141, 15211–15221.
9. Lee, Y.; Kinney, R. A.; Hoffman, B. M.; Peters, J. C. *J. Am. Chem. Soc.* **2011**, 133, 16366–16369.
10. Rittle, J.; Peters, J. C. *J. Am. Chem. Soc.* **2017**, 139, 3161–3170.
11. Chalkley, M. J.; Del Castillo, T. J.; Matson, B. D.; Peters, J. C. *J. Am. Chem. Soc.* **2018**, 140, 6122–6129. .
12. Agarwal, R. G.; Coste, S. C.; Groff, B. D.; Heuer, A. M.; Noh, H.; Parada, G. A.; Wise, C. F.; Nichols, E. M.; Warren, J. J.; Mayer, J. M. *Chem. Rev.* **2022**, 122, 1–49.
13. Tao, J.; Perdew, J. P.; Staroverov, V. N.; Scuseria, G. E. *Phys. Rev. Lett.* **2003**, 91, 146401–146404.
14. Weigend, F. *Phys. Chem. Chem. Phys.* **2006**, 8, 1057–1065.
15. Matson, B. D.; Peters, J. C. *ACS Catal.* **2018**, 8, 1448–1455.
16. Neese, F.; Wennmohs, F.; Becker, U.; Riplinger, C. *J. Chem. Phys.* **2020**, 152, 224108.
17. *Thermodynamics — ORCA tutorials 5.0 documentation.*  
[orcasoftware.de/tutorials\\_orca/prop/thermo.html](https://orcasoftware.de/tutorials_orca/prop/thermo.html) (accessed 2023-10-22).